



1 Hydrological variations of the intermediate water masses of 2 the western Mediterranean Sea during the past 20 ka inferred 3 from neodymium isotopic composition in foraminifera and 4 cold-water corals

5

6 Quentin Dubois-Dauphin¹, Paolo Montagna^{2,3}, Giuseppe Siani¹, Eric Douville⁴, Claudia
 7 Wienberg⁵, Dierk Hebbeln⁵, Zhifei Liu⁶, Nejib Kallel⁷, Arnaud Dapoigny⁴, Marie Revel⁸,
 8 Edwige Pons-Branchu⁴, Christophe Colin^{1*}

9

10 ¹Laboratoire Geosciences Paris-Sud (GEOPS), Université de Paris Sud, Université Paris-Saclay, 91405 Orsay,
 11 France.

12 ²ISMAR-CNR, via Gobetti 101, 40129 Bologna, Italy.

13 ³Lamont-Doherty Earth Observatory, Columbia University, 61 Route 9W, Palisades, NY 10964, USA

14 ⁴Laboratoire des Sciences du Climat et de l'Environnement, LSCE/IPSL, CEA-CNRS-UVSQ, Université Paris-
 15 Saclay, F-91191 Gif-sur-Yvette, France.

16 ⁵MARUM-Center for Marine Environmental Sciences, University of Bremen, Leobener Strasse, 28359 Bremen,
 17 Germany.

18 ⁶State Key Laboratory of Marine Geology, Tongji University, Shanghai 200092, China.

19 ⁷Laboratoire Georessources, Matériaux, Environnements et Changements Globaux, LR13ES23, Faculté des
 20 Sciences de Sfax, Université de Sfax, BP1171, 3000 Sfax, Tunisia.

21 ⁸Geoazur, UNS, IRD, OCA, CNRS, 250 rue Albert Einstein, 06500 Valbonne, France

22

23

24 Correspondence to: Christophe Colin (christophe.colin@u-psud.fr)

25

26

27 **Abstract.** The neodymium isotopic composition (ϵ_{Nd}) of mixed planktonic foraminifera species and
 28 scleractinian cold-water corals (CWC; *Madrepora oculata*, *Lophelia pertusa*) collected at 280-620 m water
 29 depth in the Balearic Sea, the Alboran Sea and the south Sardinian continental margin was investigated to
 30 constrain hydrological variations at intermediate depths in the western Mediterranean Sea during the last 20 ka.
 31 Planktonic (*Globigerina bulloides*) and benthic (*Cibicidoides pachyderma*) foraminifera were also analyzed for
 32 stable oxygen ($\delta^{18}\text{O}$) and carbon ($\delta^{13}\text{C}$) isotopes. The foraminiferal and coral ϵ_{Nd} values from the Balearic Sea
 33 and the Alboran Sea are comparable over the past ~13 ka, with mean values of -8.94 ± 0.26 (1 σ ; n=24) and $-$
 34 8.91 ± 0.18 (1 σ ; n=25), respectively. Before 13 ka BP, the foraminiferal ϵ_{Nd} values are slightly lower ($-$
 35 9.28 ± 0.15) and tend to reflect a higher mixing between intermediate and deep waters, characterized by more
 36 unradiogenic ϵ_{Nd} values. The slight ϵ_{Nd} increase after 13 ka BP is associated to a marked difference in the
 37 benthic foraminiferal $\delta^{13}\text{C}$ composition of intermediate and deeper depths, which started at ~16 ka BP. This
 38 suggests an earlier stratification of the water masses and a subsequent reduced contribution of unradiogenic ϵ_{Nd}
 39 from deep waters. The CWC from the Sardinia Channel show a much larger scattering of ϵ_{Nd} values, from $-$
 40 8.66 ± 0.30 to -5.99 ± 0.50 , and a lower average (-7.31 ± 0.73 ; n=19) compared to the CWC and foraminifera from
 41 the Alboran Sea and Balearic Sea, indicative of intermediate waters sourced from the Levantine basin. At the
 42 time of sapropel S1 deposition (10.2 to 6.4 ka), the ϵ_{Nd} values of the Sardinian CWC become more unradiogenic
 43 (-8.38 ± 0.47 ; n=3 at ~8.7 ka BP), suggesting a significant contribution of intermediate waters originated from the
 44 western basin. Accordingly, we propose here that western Mediterranean intermediate waters replaced the
 45 Levantine Intermediate Water (LIW), which was strongly reduced during the mid-sapropel (~8.7 ka BP). This



46 observation supports a notable change of Mediterranean circulation pattern centered on sapropel S1 that needs
47 further investigations to be confirmed.

48

49 **1. Introduction**

50 The Mediterranean Sea is a mid-latitude semi-enclosed basin, characterized by evaporation exceeding
51 precipitation and river runoff, where the inflow of fresh and relatively warm surface Atlantic water is
52 transformed into saltier and cooler (i.e. denser) intermediate and deep waters. Several studies have demonstrated
53 that the Mediterranean thermohaline circulation was highly sensitive to both the rapid climatic changes
54 propagated into the basin from high latitudes of the Northern Hemisphere (Cacho et al., 1999, 2000, 2002;
55 Moreno et al., 2002, 2005; Paterne et al., 1999; Martrat et al., 2004; Sierro et al., 2005; Frigola et al., 2007,
56 2008) and orbitally-forced modifications of the eastern Mediterranean freshwater budget mainly driven by
57 monsoonal river runoff from the south (Rohling et al., 2002; 2004; Bahr et al., 2015). A link between the
58 intensification of the Mediterranean Outflow Water (MOW) and the intensity of the Atlantic Meridional
59 Overturning Circulation (AMOC) was proposed (Cacho et al., 1999, 2000, 2001; Bigg and Wadley, 2001; Sierro
60 et al., 2005; Voelker et al., 2006) and recently supported by new geochemical data in sediments of the Gulf of
61 Cádiz (Bahr et al., 2015). In particular, it has been suggested that the intensity of the MOW and, more generally,
62 the variations of the thermohaline circulation of the Mediterranean Sea could play a significant role in triggering
63 a switch from a weakened to an enhanced state of the AMOC through the injection of saline Mediterranean
64 waters in the intermediate North Atlantic at times of weak AMOC (Rogerson et al., 2006; Voelker et al., 2006;
65 Khélifi et al., 2009). Since the Mediterranean intermediate waters, notably the Levantine Intermediate Water
66 (LIW), represent today up to 80 % in volume of the MOW (Kinder and Parilla, 1987) and are therefore a key
67 driver of MOW-derived salt into the North Atlantic, it is crucial to gain a more complete understanding of the
68 variability of the Mediterranean intermediate circulation in the past and its impact on the outflow.

69 Previous studies have mainly focused on the glacial variability of the deep-water circulation in the western
70 Mediterranean basin (Cacho et al., 2000, 2006; Sierro et al., 2005; Frigola et al., 2007, 2008). During the Last
71 Glacial Maximum (LGM), strong deep-water convection took place in the Gulf of Lions, producing cold, well-
72 ventilated western Mediterranean Deep Water (WMDW) (Cacho et al., 2000, 2006; Sierro et al., 2005), while
73 the MOW flowed at greater depth in the Gulf of Cádiz (Rogerson et al., 2005; Schönfeld and Zahn, 2000). With
74 the onset of the Termination 1 (T1) at about 15 ka, the WMDW production declined until the transition to the
75 Holocene due to the rising sea level, with a relatively weak mode during the Heinrich Stadial 1 (HS1) and the
76 Younger Dryas (YD) (Sierro et al., 2005; Frigola et al., 2008), that led to the deposition of the Organic Rich
77 Layer 1 (ORL1; 14.5-8.2 ka BP; Cacho et al., 2002).

78 Because of the disappearance during the Early Holocene of specific epibenthic foraminiferal species, such as
79 *Cibicidoides* spp., which are commonly used for paleohydrological reconstructions, information about the
80 Holocene variability of the deep-water circulation in the western Mediterranean are relatively scarce and are
81 mainly based on grain size analysis and sediment geochemistry (Frigola et al., 2007). These authors have
82 identified four distinct phases representing different deep-water overturning conditions in the western
83 Mediterranean basin during the Holocene, as well as centennial- to millennial-scale abrupt events of overturning
84 reinforcement.



85 Faunal and stable isotope records from benthic foraminifera located at intermediate depths in the eastern basin
86 reveal uninterrupted well-ventilated LIW during the last glacial period and deglaciation (Kuhnt et al., 2008;
87 Schmiedl et al., 2010). A grain-size record obtained from a sediment core collected within the LIW depth range
88 (~500 m water depth) at the east Corsica margin also reveals enhanced bottom currents during HS1 and the YD
89 (Toucanne et al., 2012). The Early Holocene is characterized by a collapse of the LIW (Kuhnt et al., 2008;
90 Schmiedl et al., 2010; Toucanne et al., 2012) synchronous with the sapropel S1 deposition (10.2 – 6.4 cal ka BP;
91 Mercone et al., 2000). Proxies for deep-water conditions reveal the occurrence of episodes of deep-water
92 overturning reinforcement in the eastern Mediterranean basin at 8.2 ka BP (Rohling et al., 1997, 2015; Kuhnt et
93 al., 2007; Abu-Zied et al., 2008; Siani et al., 2013; Tachikawa et al.; 2015), responsible for the interruption of the
94 sapropel S1 in the eastern Mediterranean basin (Mercone et al., 2001; Rohling et al., 2015).

95 It has recently been shown that the neodymium (Nd) isotopic composition, expressed as $\varepsilon\text{Nd} =$
96 $([({}^{143}\text{Nd}/{}^{144}\text{Nd})_{\text{sample}} / ({}^{143}\text{Nd}/{}^{144}\text{Nd})_{\text{CHUR}}] - 1) \times 10000$ (CHUR: Chondritic Uniform Reservoir [Jacobsen and
97 Wasserburg , 1980]) of living and fossil scleractinian CWC faithfully traces intermediate and deep-water mass
98 provenance and mixing of the ocean (e.g. van de Flierdt et al., 2010; Colin et al., 2010; López Correa et al.,
99 2012; Monterro-Serrano et al., 2011, 2013; Copard et al., 2012). Differently from the CWC, the εNd
100 composition of fossil planktonic foraminifera is not related to the ambient seawater at calcification depths but
101 reflects the bottom and/or pore water εNd , due to the presence of authigenic Fe-Mn coatings precipitated on their
102 carbonate shell (Roberts et al., 2010; Elmore et al., 2011; Piotrowski et al., 2012; Tachikawa et al., 2014; Wu et
103 al., 2015). Therefore, the εNd composition of planktonic foraminiferal tests can be used as a useful tracer of
104 deep-water circulation changes in the past, although the effect of pore water on foraminiferal εNd values could
105 potentially complicate the interpretation (Tachikawa et al., 2014).

106 In the Mediterranean Sea, modern seawater εNd values display a large range from ~-11 to ~-5, and a clear
107 vertical and longitudinal gradient, with more radiogenic values encountered in the eastern basin and typically at
108 intermediate and deeper depths (Spivack and Wasserburg 1988; Henry et al., 1994; Tachikawa et al., 2004;
109 Vance et al., 2004). Considering this large εNd contrast, εNd recorded in fossil CWC and planktonic
110 foraminifera from the Mediterranean offers great potential to trace intermediate and deep-water mass exchange
111 between the two basins, especially during periods devoid of key epibenthic foraminifera, such as the sapropel S1
112 and ORL1 events.

113 Here, the εNd of planktonic foraminifera from a sediment core collected in the Balearic Sea and CWC samples
114 from the Alboran Sea and the Sardinia Channel was investigated to establish past changes of the εNd values at
115 intermediate depths and constrain hydrological variations of the LIW during the past ~20 ka. The εNd values
116 have been combined with stable oxygen ($\delta^{18}\text{O}$) and carbon ($\delta^{13}\text{C}$) isotope measurements of benthic (*Cibicidoides*
117 *pachyderma*) and planktonic (*Globigerina bulloides*) foraminifera and sea-surface temperature estimates by
118 modern analogue technique (MAT). Results reveal significant changes of the E-W gradient of εNd values for the
119 LIW of the western basin interpreted by a drastic reduction of the hydrological exchanges between the western
120 and eastern Mediterranean Sea and the subsequent higher proportion of intermediate water produced in the Gulf
121 of Lions during the time interval corresponding to the sapropel S1 deposition.

122

123

124



125

2. Seawater ϵ Nd distribution in the Mediterranean Sea

126 The Atlantic Water (AW) enters the Mediterranean Sea as surface inflow through the Strait of Gibraltar with an
 127 unradiogenic ϵ Nd signature of \sim 9.7 in the strait (Tachikawa et al., 2004) and \sim 10.4 in the Alboran Sea
 128 (Tachikawa et al., 2004, Spivack and Wasserbürg, 1988) for depths shallower than 50 m. During its eastward
 129 flowing, AW mixes with upwelled Mediterranean Intermediate Water forming the Modified Atlantic Water
 130 (MAW) that spreads within the basin (Millot and Taupier-Letage, 2005) (Fig.1). The surface water ϵ Nd values
 131 (shallower than 50 m) range from -9.8 to -8.8 in the western Mediterranean basin (Henry et al., 1994; Montagna
 132 et al., in prep) and -9.3 to -4.2 in the eastern basin, with seawater off the Nile delta showing the most radiogenic
 133 values (Tachikawa et al., 2004; Vance et al., 2004; Montagna et al., in prep). The surface waters in the eastern
 134 Mediterranean basin become denser due to strong mixing and evaporation caused by cold and dry air masses
 135 flowing over the Cyprus-Rhodes area in winter, and eventually sink leading to the formation of LIW
 136 (Ovchinnikov, 1984; Lascaratos et al., 1993, 1998; Malanotte-Rizzoli et al., 1999; Pinardi and Masetti, 2000).
 137 The LIW spreads throughout the entire Mediterranean basin at depths between \sim 150-200 m and \sim 600-700 m,
 138 and is characterized by more radiogenic ϵ Nd values ranging from -7.9 to -4.8 (average value \pm 1 σ : -6.6 \pm 1) in
 139 the eastern basin and from -10.4 to -7.58 (-8.7 \pm 0.9) in the western basin (Henry et al., 1994; Tachikawa et al.,
 140 2004; Vance et al., 2004; Montagna et al., in prep). The LIW acquires its ϵ Nd signature mainly from the partial
 141 dissolution of Nile River particles (Tachikawa et al., 2004), which have an average isotopic composition of -3.25
 142 (Weldeab et al., 2002), and the mixing along its path with overlying and underlying water masses with different
 143 ϵ Nd signatures. The LIW finally enters the Atlantic Ocean at intermediate depths through the Strait of Gibraltar
 144 with an average ϵ Nd value of -9.2 ± 0.2 (Tachikawa et al., 2004; Montagna et al., in prep).
 145 The WMDW is formed in the Gulf of Lions due to winter cooling and evaporation followed by mixing between
 146 the relative fresh surface water and the saline LIW and spreads into the Balearic basin and Tyrrhenian Sea
 147 between \sim 2000 m and 3000 m (Millot, 1999; Schroeder et al., 2013) (Fig. 1). The WMDW is characterized by an
 148 average ϵ Nd value of -9.4 ± 0.9 (Henry et al., 1994; Tachikawa et al., 2004; Montagna et al., in prep). Between
 149 the WDMW and the LIW (from \sim 700 to 2000 m), the Tyrrhenian Deep Water (TDW) has been found (Millot et
 150 al., 2006), which is produced by the mixing between WMDW and Eastern Mediterranean Deep Water (EMDW)
 151 that cascades in the Tyrrhenian Sea after entering from the Strait of Sicily (Millot, 1999, 2009; Astraldi et al.,
 152 2001). The TDW has an average ϵ Nd value of -8.1 ± 0.5 (Montagna et al., in prep).
 153

154

3. Material and methods

3.1. Cold-water coral and foraminifera samples

155 Forty-four CWC samples belonging to the species *Lophelia pertusa* and *Madrepora oculata* collected from the
 156 Alboran Sea and the Sardinia Channel were selected for this study (Fig. 1). Nineteen fragments were collected at
 157 various core depths from a coral-bearing sediment core (RECORD 23; $38^{\circ}42.18' N$; $08^{\circ}54.75' E$; Fig. 1)
 158 retrieved from 414 m water depth in the "Sardinian Cold-Water Coral Province" (Taviani et al., 2015) during the
 159 R/V Urania cruise "RECORD" in 2013. The Sardinian CWC samples were used for U-series dating and Nd
 160 isotopic composition measurements. For the southern Alboran Sea, twenty-five CWC samples were collected at
 161 water depths between 280 and 442 m in the "eastern Melilla Coral Province" (Fig. 1) during the R/V Poseidon
 162 cruise "POS-385" in 2009 (Hebbeln et al. 2009). Eleven samples were collected at the surface of two coral
 163 mounds (New Mound and Horse Mound) and three coral ridges (Brittlestar ridges I, II and III), using a box corer
 164



165 and a remotely operated vehicle (ROV). In addition, fourteen CWC samples were collected from various core
166 depths of three coral-bearing sediment cores (GeoB13728, 13729 and 13730) retrieved from the Brittlestar ridge
167 I. Details on the location of surface samples and cores collected in the southern Alboran Sea and details on the
168 radiocarbon ages obtained from these coral samples are reported in Fink et al. (2013). Like the CWC sample set
169 from the Sardinia Channel, the dated Alboran CWC samples were also used for further Nd isotopic composition
170 analyses in this study.

171 In addition, a sediment core (barren of any CWC fragments) was recovered in the Balearic Sea at 622 m water
172 depth during the R/V Le Suroît cruise "PALEOCINAT II" in 1992 (SU92-33; 35°25.38' N; 0°33.86' E; Fig. 1).
173 The core was sub-sampled continuously at 5-10 cm intervals for the upper 2.1 m for a total number of 24
174 samples used for further multi-proxy analyzes.

175

176 **3.2. Analytical procedures on cold-water coral samples**

177 **3.2.1. U/Th dating**

178 The nineteen CWC samples collected from the sediment core RECORD 23 (Sardinia Channel) were analysed for
179 uranium and thorium isotopes to obtain absolute dating using a Thermo Scientific™ Neptune^{Plus} MC-ICPMS
180 installed at the Laboratoire des Sciences du Climat et de l'Environnement (LSCE, Gif-sur-Yvette, France). Prior
181 to analysis, the samples were carefully cleaned using a small diamond blade to remove any visible contamination
182 and sediment-filled cavities. The fragments were examined under a binocular microscope to ensure against the
183 presence of bioeroded zones and finally crushed into a coarse-grained powder with an agate mortar and pestle.
184 The powders (~60-100 mg) were transferred to acid cleaned Teflon beakers, ultrasonicated in MilliQ water,
185 leached with 0.1N HCl for ~ 15 s and finally rinsed twice with MilliQ water. The physically and chemically
186 cleaned samples were dissolved in 3-4 ml dilute HCl (~10%) and mixed with an internal triple spike with known
187 concentrations of ²²⁹Th, ²³³U and ²³⁶U, calibrated against a Harwell Uraninite solution (HU-1) assumed to be at
188 secular equilibrium. The solutions were evaporated to dryness at 70°C, redissolved in 0.6 ml 3N HNO₃ and then
189 loaded into 500 µl columns packed with Eichrom UTEVA resin to isolate uranium and thorium from the other
190 major and trace elements of the carbonate matrix. The U and Th separation and purification followed a
191 procedure slightly modified from Douville et al. (2010). The U and Th isotopes were determined following the
192 protocol recently revisited at LSCE (Pons-Branchu et al., 2014). The ²³⁰Th/U ages were calculated from
193 measured atomic ratios through iterative age estimation (Ludwig and Titterington, 1994), using the ²³⁰Th, ²³⁴U
194 and ²³⁸U decay constants of Cheng et al. (2013) and Jaffey et al. (1971). Due to the low ²³²Th concentration (< 1
195 ng/g; see Table 1), no correction was applied for the non-radiogenic ²³⁰Th fraction.

196

197 **3.2.2 Nd isotopic composition analyses on cold-water coral fragments**

198 Sub-samples of the CWC fragments from the Sardinia Channel used for U-series dating in this study (Table 1) as
199 well as sub-samples of the twenty-five CWC fragments originating from the Alboran Sea, which were already
200 radiocarbon-dated by Fink et al. (2013) (Table 2), were used for further Nd isotopic composition analyses. The
201 fragments (350 to 600 mg) were subjected to a mechanical and chemical cleaning procedure. The visible
202 contaminations, such as Fe-Mn coatings and detrital particles, were carefully removed from the inner and
203 outermost surfaces of the coral skeletons using a small diamond blade. The physically cleaned fragments were
204 ultrasonicated for 10 min with 0.1 N ultra-clean HCl, followed by several MilliQ water rinses and finally



205 dissolved in 2.5 N ultraclean HNO₃. Nd was separated from the carbonate matrix using Eichrom TRU and LN
206 resins, following the analytical procedure described in detail in Copard et al. (2010).
207 The ¹⁴³Nd/¹⁴⁴Nd ratios of all purified Nd fractions were analyzed using the ThermoScientific Neptune^{Plus} Multi-
208 Collector Inductively Coupled Plasma Mass Spectrometer (MC-ICP-MS) hosted at LSCE. The mass-
209 fractionation correction was made by normalizing ¹⁴⁶Nd/¹⁴⁴Nd to 0.7219 and applying an exponential law.
210 During each analytical session, samples were systematically bracketed with analyses of JNd-1 and La Jolla
211 standard solutions, which are characterised by accepted values of 0.512115±0.000006 (Tanaka et al., 2000) and
212 0.511855±0.000007 (Lugmair et al., 1983), respectively. Standard JNd-1 and La Jolla solutions were analysed
213 at concentrations similar to those of the samples (5-10 ppb) and all the measurements affected by instrumental
214 bias were corrected, when necessary, using La Jolla standard. The external reproducibility (2σ) for time resolved
215 measurement, deduced from repeated analyses of La Jolla and JNd-1 standards, ranged from 0.1 to 0.5 εNd
216 units for the different analytical sessions. The analytical error for each sample analysis was taken as the external
217 reproducibility of the La Jolla standard for each session. Concentrations of Nd blanks were negligible compared
218 to the amount of Nd of CWC investigated in this study.

219

220 3.3. Analyses on sediment of core SU92-33

221 3.3.1. Radiocarbon dating

222 Radiocarbon dating was measured at UMS-ARTEMIS (Pelletron 3MV) AMS (CNRS-CEA Saclay, France).
223 Seven AMS radiocarbon (¹⁴C) dating were performed in core SU92-33 on well-preserved calcareous tests of the
224 planktonic foraminifera *G. bulloides* in the size fraction >150 µm (Table 3). The age model for the core was
225 derived from the calibrated planktonic ages by applying a mean reservoir effect of ~400 years (Siani et al., 2000,
226 2001). All ¹⁴C ages were converted to calendar years (cal. yr BP, BP = AD 1950) by using the INTCAL13
227 calibration data set (Reimer et al., 2013) and the CALIB 7.0 program (Stuiver and Reimer, 1993).

228

229 3.3.2. Stable isotopes

230 Stable oxygen ($\delta^{18}\text{O}$) and carbon ($\delta^{13}\text{C}$) isotope measurements were performed in core SU92-33 on well-
231 preserved (clean and intact) samples of the planktonic foraminifera *G. bulloides* (250–315 µm fraction) and the
232 epibenthic foraminifera *C. pachyderma* (250–315 µm fraction) using a Finnigan MAT-253 mass spectrometer at
233 the State Key Laboratory of Marine Geology (Tongji University). Both $\delta^{18}\text{O}$ and $\delta^{13}\text{C}$ values are presented
234 relative to the Pee Dee Belemnite (PDB) scale by comparison with the National Bureau of Standards (NBS) 18
235 and 19. The mean external reproducibility was checked by replicate analyses of laboratory standards and is better
236 than ±0.07‰ (1σ) for $\delta^{18}\text{O}$ and ±0.04‰ for $\delta^{13}\text{C}$.

237

238 3.3.3 Nd isotope measurements on planktonic foraminifera

239 Approximately 25 mg of mixed planktonic foraminifera species were picked from the >63 µm size fraction of
240 each sample already used for stable isotope measurements (Table 4). The samples were gently crushed between
241 glass slides under the microscope to ensure that all chambers were open, and ultrasonicated with MilliQ water.
242 Samples were allowed to settle between ultrasonication steps before removing the supernatant. Each sample was
243 rinsed thoroughly with MilliQ water until the solution was clear and free of clay. The cleaned samples were
dissolved in 1N acetic acid and finally centrifuged to ensure that all residual particles were removed, following



244 the procedure described in Roberts et al. (2010). Nd was separated following the analytical procedure reported in
245 Wu et al. (2015). For details on the measurement of Nd isotopes see the section above.

246

247 *3.3.4. Modern analogue technique (MAT)*

248 The palaeo-sea surface temperatures (SST) were estimated using the modern analogue technique (MAT)
249 (Hutson, 1980; Prell, 1985), implemented by Kallel et al. (1997) for the Mediterranean Sea. This method directly
250 measures the difference between the faunal composition of a fossil sample with a modern database, and it
251 identifies the best modern analogues for each fossil assemblage (Prell, 1985). Reliability of SST reconstructions
252 is estimated using a square chord distance test (dissimilarity coefficient), which represents the mean degree of
253 similarity between the sample and the best 10 modern analogues. When the dissimilarity coefficient is lower than
254 0.25, the reconstruction is considered to be of good quality (Overpeck et al., 1985; Kallel et al., 1997). For core
255 SU92-33, good dissimilarity coefficients are <0.2, with an average value of 0.13.

256

257 **4. Results**

258 **4.1. Cold-water coral ages**

259 The good state of preservation for the CWC samples from the Sardinia Channel (RECORD 23; Fig. 1) is attested
260 by their initial $\delta^{234}\text{U}$ values (Table 1), which is in the range of the modern seawater value (146.8 ± 0.1 ; Andersen
261 et al., 2010). If the uncertainty of the $\delta^{234}\text{U}_i$ is taken into account, all the values fulfill the so-called “strict” ± 4
262 % reliability criterion and the U/Th ages can be considered strictly reliable. The coral ages range from
263 0.091 ± 0.011 to 10.904 ± 0.042 ka BP (Table 1), and reveal three distinct clusters of coral age distribution during
264 the Holocene representing periods of sustained coral occurrence. These periods coincide with the Early Holocene
265 encompassing a 700-years-lasting time interval from ~10.9 to 10.2 ka BP, the very late Early Holocene at ~8.7
266 ka BP, and the Late Holocene starting at ~1.5 ka BP (Table 1).

267

268 Radiocarbon ages obtained for CWC samples collected in the Alboran Sea were published by Fink et al. (2013)
269 (Table 2). They also document three periods of sustained CWC occurrence coinciding with the Bølling–Allerød
270 (B-A) interstadial (13.5–12.9 cal ka BP), the Early Holocene (11.2–9.8 cal ka BP) and the Mid- to Late Holocene
271 (5.4–0.3 cal ka BP).

272

273 **4.2 Chronological framework for core SU92-33**

274 The stratigraphy of core SU92-33 was derived from the $\delta^{18}\text{O}$ variations of the planktonic foraminifera
275 *G. bulloides* (Fig. 2b). The last glacial/interglacial transition and the Holocene encompasses the upper 2.1 m of
276 the core (Fig. 2b). The $\delta^{18}\text{O}$ record of *G. bulloides* shows higher values (~3.5 %) during the late glacial
277 compared to the Holocene (from ~1.5 to 0.8 %) exhibiting a pattern similar to those observed in nearby deep-sea
278 cores from the Western Mediterranean Sea (Sierro et al., 2005; Melki et al., 2009).

279

280 The age model of core SU92-33 is based on 7 AMS- ^{14}C age measurements for the upper 1.2 m of the core
281 and by a linear interpolation between these ages (Table 3, Fig. 2). Below, a control point has been established for
282 the onset of the last deglaciation that presents a coeval age in the western and central Mediterranean Sea at about
283 17 cal ka BP (Sierro et al., 2005; Melki et al., 2009; Siani et al., 2001). The upper 2.1 m of core SU92-33 spans
284 the last 19 ka, with an estimated average sedimentation rate between 9 to 15 cm ka^{-1} , with the lowest values
285 observed during the Holocene.



284

285 **4.3 SST reconstructions of core SU92-33**

286 April-May SST reconstruction was derived from MAT to define the main climatic events recorded in
287 core SU92-33 during the last 19 ka. SSTs vary from 8.5°C to 17.5°C with high amplitude variability over the last
288 19 ka BP (Fig. 2a). The LGM (19–18 ka BP) is characterized by SST values centered at around 12°C. Then, a
289 progressive decrease of ~4°C between 17.8 ka to 16 ka marks the Heinrich Stadial 1 (HS1) (Fig. 2a). A warming
290 phase (~14°C) between 14.5 ka BP and 13.8 ka BP coincides with the B-A interstadial and is followed by a
291 cooling (~11°C) between 13.1 ka BP and 11.8 ka BP largely corresponding to the YD (Fig. 2). During the
292 Holocene, SSTs show mainly values of ~16°C, with one exception between 7 ka BP and 6 ka BP pointing to an
293 abrupt cooling of ~3°C (Fig. 2a). From the late glacial to the Holocene, SST variations show a similar pattern to
294 that previously observed in the Gulf of Lions and Tyrrhenian Sea (Kallel et al., 1997; Melki et al., 2009) and
295 globally synchronous for the main climatic transitions to the well dated South Adriatic Sea core MD90-917
296 confirming the robustness of the SU92-33 age model (Fig. 2a).

297

298 **4.4 Benthic stable oxygen and carbon isotope records of core SU92-33**

299 The $\delta^{18}\text{O}$ and $\delta^{13}\text{C}$ records obtained from the benthic foraminifera *C. pachyderma* display significant variations
300 at millennial time scales (Figs. 2c and 2d). The $\delta^{18}\text{O}$ values decrease steadily from ~4.5 ‰ during the LGM to
301 ~1.5 ‰ during the Holocene, without showing any significant excursion during HS1 and the YD events (Fig.
302 2c), in agreement with results obtained for the neighbor core MD99-2343 (Sierro et al., 2005).

303 The $\delta^{13}\text{C}$ record obtained from *C. pachyderma* shows a decreasing trend since the LGM with a low variability
304 from ~1.6 ‰ to ~0.6 ‰ (Fig. 2d). The heaviest $\delta^{13}\text{C}$ values are related to the LGM (~1.6 ‰) while the lightest
305 values (~0.6 ‰) characterize the Early Holocene and in particular the period corresponding to the sapropel S1
306 event in the eastern Mediterranean basin (Fig. 2d).

307

308 **4.5 Nd isotopic composition of planktonic foraminifera and cold-water corals**

309 ϵNd values of planktonic foraminifera of core SU92-33 collected from the Balearic Sea vary within a relatively
310 narrow range between -9.50 ± 0.30 and -8.61 ± 0.30 , with an average value of -9.06 ± 0.28 (Table 2, Fig. 3b). The
311 record shows a slight increasing trend since the LGM, with the more unradiogenic values (average -9.28 ± 0.15 ;
312 n=7) observed in the oldest part of the record (between 18 and 13.5 ka BP), whereas Holocene values are
313 generally more radiogenic (average -8.84 ± 0.22 ; n=17) (Fig. 3b).

314 The ϵNd record obtained for the CWC samples from the Alboran Sea displays a narrow range from -9.22 ± 0.30 to
315 -8.59 ± 0.3 , which is comparable to the ϵNd record obtained on planktonic foraminifera from the Balearic Sea
316 over the last 13.5 ka (Table 2, Fig. 3b). Most of the CWC ϵNd values are similar within error and the record does
317 not reveal any clear difference over the last ~13.5 ka.

318 Finally, the CWC samples from the Sardinia Channel display ϵNd values ranging from -5.99 ± 0.50 to -7.75 ± 0.10
319 during the Early and Late Holocene, and values as low as -8.66 ± 0.30 during the mid-sapropel S1 deposition
320 (S1a) (~8.7 ka BP) (Table 1, Fig. 3c).

321

322

323



324

5. Discussion

325 As first observations, the CWC and foraminiferal ϵ_{Nd} values measured for this study indicate a pronounced
 326 dispersion at intermediate depth in terms of absolute values and variability in Nd isotopes during the Holocene
 327 between the Alboran and Balearic Seas and the Sardinia Channel. In addition the foraminiferal ϵ_{Nd} record
 328 reveals an evolution towards more radiogenic values at intermediate water depth in the Balearic Sea over the last
 329 ~19 ka (Fig. 3).

330 A prerequisite to properly interpret such ϵ_{Nd} values differences and variations through time consists in
 331 characterizing the present-day ϵ_{Nd} of the main water-mass end-members circulating in the western
 332 Mediterranean basin. This is possible by evaluating the temporal changes in ϵ_{Nd} of the end-members since the
 333 LGM, and assessing the potential influences of lithogenic Nd input and regional exchange between the
 334 continental margins and seawater (“boundary exchange”; Lacan and Jeandel, 2001, 2005) on the ϵ_{Nd} values of
 335 intermediate water masses.

336 During its westward flow, the LIW continuously mixes with surrounding waters with different ϵ_{Nd} signatures
 337 lying above and below. For the western Mediterranean basin, these water masses are the MAW/Western
 338 Intermediate Water (WIW) and the TDW/WMDW, respectively. Accordingly, a well-defined and gradual ϵ_{Nd}
 339 gradient exists at intermediate depth between the eastern and western Mediterranean basins, with LIW values
 340 becoming progressively more unradiogenic towards the Strait of Gibraltar, from -4.8 ± 0.2 at 227 m in the
 341 Levantine basin to -10.4 ± 0.2 at 200 m in the Alboran Sea (Tachikawa et al., 2004). Such an ϵ_{Nd} pattern implies
 342 an effective vertical mixing with more unradiogenic water masses along the E-W LIW trajectory ruling out
 343 severe isotopic modifications of the LIW due to the local exchange between the continental margins and
 344 seawater. Unfortunately, no information exists on the potential temporal variability in ϵ_{Nd} of the Mediterranean
 345 water-mass end-members since the LGM.

346 It has been demonstrated that eolian dust input can modify the surface and sub-surface ϵ_{Nd} distribution of the
 347 ocean in some areas (Arsouze et al., 2009). The last glacial period was associated with an aridification of North
 348 Africa (Sarnthein et al., 1981; Hooghiemstra et al., 1987; Moreno et al., 2002; Wienberg et al., 2010) and higher
 349 fluxes of Saharan dust to the NE tropical Atlantic (Itambi et al., 2009) and the western Mediterranean Sea
 350 characterized by unradiogenic ϵ_{Nd} values (between -10 ± 0.4 and -17 ± 0.4 ; Grousset et al., 1992, 1998; Grousset
 351 and Biscaye, 2005). Bout-Roumazeilles et al. (2013) documented a dominant role of eolian supply in the Siculo-
 352 Tunisian Strait during the last 20 ka, with the exception of a significant riverine contribution (from the Nile
 353 River) and a strong reduction of eolian input during the sapropel S1 event. Such variations in the eolian input to
 354 the Mediterranean Sea are not associated to a significant change in the seawater ϵ_{Nd} record obtained for the
 355 Balearic Sea (core SU92-33) during the sapropel S1 event (Fig. 3). Furthermore, the ϵ_{Nd} signature of the CWC
 356 from the Sardinia Channel (core RECORD 23) shifts to more unradiogenic values (-8.66 ± 0.30) during the
 357 sapropel S1 event, which is opposite to what expected if related to a strong reduction of eolian sediment input.
 358 Thus, these results suggest that changes of eolian dust input since the LGM were not responsible for the
 359 observed ϵ_{Nd} variability at intermediate water depths.

360 Consequently, assuming that the Nd isotopic budget of the western Mediterranean Sea has not been strongly
 361 modified since the LGM, the reconstructed variations of the E-W gradient of ϵ_{Nd} values in the western
 362 Mediterranean Sea for the past and notably during the sapropel S1 event (Fig. 3) are indicative of a major
 363 reorganization of intermediate water circulation.



364

365 5.1 Hydrological changes in the Alboran and Balearic Seas since the LGM

366 The range in ϵ Nd for the CWC from the Alboran Sea (from -9.22 ± 0.30 to $-8.8.59 \pm 0.30$; Table 2) is very close to
367 the one obtained for the planktonic foraminifera from the Balearic Sea (from -9.50 ± 0.3 to -8.61 ± 0.3 ; Table 4,
368 Fig. 3c), suggesting that both sites are influenced by the same intermediate water masses at least for the last 13.5
369 ka BP. Today, LIW occupies a depth range between ~200 and ~700 m in the western Mediterranean basin
370 (Millot, 1999; Sparnacchia et al., 1999). More specifically, the salinity maximum corresponding to the core of
371 LIW is found at around 400 m in the Alboran Sea (Millot, 2009) and up to 550 m in the Balearic Sea (López-
372 Jurado et al., 2008). The youngest CWC sample collected in the Alboran Sea with a rather "recent" age of 0.34
373 cal ka BP (Fink et al. 2013) displays an ϵ Nd value of -8.59 ± 0.30 (Table 2) that is similar to the present-day value
374 of the LIW at the same site (-8.3 ± 0.2) (Dubois-Dauphin et al., submitted) and is significantly different from the
375 WMDW ϵ Nd signature in the Alboran Sea (-10.7 ± 0.2 , 1270 m water depth; Tachikawa et al., 2004). Considering
376 the intermediate depth range of the studied CWC and foraminifera samples, we can reasonably assume that
377 samples from both sites, in the Balearic Sea (622 m water depth) and in the Alboran Sea (280 to 442 m water
378 depth), record ϵ Nd variations of the LIW. The ϵ Nd record obtained on planktonic foraminifera generally displays
379 more unradiogenic and homogenous values before ~13 cal ka BP (range: -9.46 to -9.12) compared to the most
380 recent part of the record (range: -9.50 to -8.61), with the highest value of -8.61 ± 0.3 in the Early and Late
381 Holocene.
382 The $\delta^{18}\text{O}$ record obtained on *G. bulloides* indicates an abrupt 1‰ excursion towards lighter values centered at
383 about 16 cal ka BP (Table 4), synchronous with the HS1 (Fig. 2b), which is similar to the $\delta^{18}\text{O}$ shift reported by
384 Sierro et al. (2005) for a core collected at 2391 m water depth NE of the Balearic Islands (MD99-2343; Fig. 1).
385 As the Heinrich events over the last glacial period are characterized by colder and fresher surface water in the
386 Alboran Sea (Cacho et al., 1999; Pérez-Folgado et al., 2003; Martrat et al., 2004) and dry climate on land over
387 the western Mediterranean Sea (Allen et al., 1999; Combourieu-Nebout et al., 2002; Sanchez Goni et al., 2002;
388 Bartov et al., 2003), lighter $\delta^{18}\text{O}$ values of planktonic *G. bulloides* are thought to be the result of the inflow of
389 freshwater derived from the melting of icebergs in the Atlantic Ocean into the Mediterranean Sea (Sierro et al.,
390 2005; Rogerson et al., 2008).
391 During this time interval, the $\delta^{13}\text{C}$ record of *C. pachyderma* from the Balearic Sea (core SU92-33) displays a
392 decreasing $\delta^{13}\text{C}$ trend after ~16 cal ka BP (from 1.4 ‰ to 0.9 ‰; Table 4; Fig. 4a). Moreover, the $\delta^{13}\text{C}$ record
393 obtained on benthic foraminifera *C. pachyderma* from the deep Balearic Sea (core MD99-2343) reveals similar
394 $\delta^{13}\text{C}$ values before ~16 cal ka BP suggesting well-mixed and ventilated water masses during the LGM and the
395 onset of the deglaciation (Sierro et al., 2005).
396 The slightly lower foraminiferal ϵ Nd values before ~13 cal ka BP could reflect a stronger influence of water
397 masses deriving from the Gulf of Lions as WMDW (ϵ Nd: -9.4 ± 0.9 ; Henry et al., 1994; Tachikawa et al., 2004;
398 Montagna et al., in prep). This is in agreement with ϵ Nd results obtained by Jiménez-Espejo et al. (2015) from
399 planktonic foraminifera collected from deep-water sites (1989 m and 2382 m) in the Alboran Sea (Fig. 4c).
400 Jiménez-Espejo et al. (2015) documented lower ϵ Nd values (ranging from -10.14 ± 0.27 to -9.58 ± 0.22) during the
401 LGM, suggesting an intense deep-water formation. This is also associated to an enhanced activity of the deeper
402 branch of the MOW in the Gulf of Cádiz (Rogerson et al., 2005; Voelker et al., 2006) linked to the active
403 production of the WMDW in the Gulf of Lions during the LGM (Jiménez-Espejo et al., 2015).



404 The end of the HS1 (14.7 cal ka BP) is concurrent with the onset of the B-A warm interval characterized by
405 increased SST identified for various sites in the Mediterranean Sea (Cacho et al., 1999; Martrat et al., 2004;
406 Essallami et al., 2007), in agreement with the SST record obtained for the Balearic Sea (SU92-33: Fig. 3a). The
407 B-A interval is associated to the so-called melt-water pulse 1A (e.g. Weaver et al., 2003) occurring at around
408 14.5 cal ka BP. This led to a rapid sea-level rise of about 20 m in less than 500 years and large freshwater
409 discharges in the Atlantic Ocean due to the melting of continental ice sheets (Deschamps et al., 2012), resulting
410 in an enhanced Atlantic inflow across the Strait of Gibraltar. Synchronously, cosmogenic dating of Alpine
411 glacier retreat throughout the western Mediterranean hinterland suggests maximum retreat rates (Ivy-Ochs et al.,
412 2007; Kelly et al., 2006). Overall, these events are responsible for freshening Mediterranean waters and reduced
413 surface water density, and hence, weakened ventilation of intermediate (Toucanne et al., 2012) and deep-water
414 masses (Cacho et al., 2000; Sierro et al., 2005). Similarly, lower benthic $\delta^{13}\text{C}$ values obtained for the Balearic
415 Sea (Fig. 4a) point to less ventilated intermediate water relative to the late glacial. In addition, a decoupling in
416 the benthic $\delta^{13}\text{C}$ values is observed between deep (MD99-2343) and intermediate (core SU92-33) waters after
417 ~16 cal ka BP (Sierro et al. 2005), suggesting an enhanced stratification of the waters masses (Fig. 4a). At this
418 time, the shallowest ϵNd record from the deep Alboran Sea (core 300G) shifted towards more radiogenic values,
419 while the deepest one (core 304G) remained close to the LGM values (Jimenez-Espejo et al., 2015) (Fig. 4c).
420 Furthermore, results from the UP10 fraction (particles $> 10 \mu\text{m}$) of the MD99-2343 sediment core (Fig. 4d),
421 indicate a declining bottom-current velocity at 15 ka (Frigola et al., 2008). Rogerson et al. (2008) have
422 hypothesized that during deglacial periods the sinking depth of dense waters produced in the Gulf of Lions was
423 shallower resulting in new intermediate water (WIW) rather than new deep-water (WMDW) as observed today
424 during mild winters (Millot, 1999; Schott et al., 1996). Therefore, intermediate depths of the Balearic Sea could
425 have been isolated from the deep-water with the onset of the T1 (at ~15 ka BP). The reduced convection in the
426 deep western Mediterranean Sea together with the shoaling of the nutricline (Rogerson et al., 2008) led to the
427 deposition of the ORL 1 (14.5 to 8.2 ka B.P.; Cacho et al., 2002) and dysoxic conditions below 2000 m in
428 agreement with the absence of epibenthic foraminifera such as *C. pachyderma* after 11 cal ka BP in MD99-2343
429 (Sierro et al., 2005) (Fig. 4a).
430 After 13.5 ka BP, planktonic foraminifera ϵNd values from the Balearic Sea (core SU92-33) become more
431 radiogenic and are in the range of CWC ϵNd values from the Alboran Sea (Fig. 4b). These values may reveal a
432 stronger influence of the LIW in the Balearic Sea during the Younger Dryas, as also supported by the sortable
433 silt record from the Tyrrhenian Sea (Toucanne et al., 2012) (Fig. 4e). Deeper depths of the Alboran Sea also
434 record a stronger influence of the LIW with an ϵNd value of -9.1 ± 0.4 (Jimenez-Espejo et al., 2015). In addition,
435 a concomitant activation of the upper MOW branch, as reconstructed from higher values of Zr/Al ratio in
436 sediments of the Gulf of Cádiz, can be related to the enhanced LIW flow in the western Mediterranean Sea (Fig.
437 4f) (Bahr et al., 2015).
438 The time of sapropel S1 deposition (10.2 – 6.4 ka) is characterized by a weakening or a shutdown of
439 intermediate- and deep-water formation in the eastern Mediterranean basin (Rossignol-Strick et al., 1982; Cramp
440 and O'Sullivan, 1999; Emeis et al., 2000; Rohling et al., 2015). At this time, planktonic foraminifera ϵNd values
441 from intermediate water depths in the Balearic Sea (core SU92-33) remain high (between -9.15 ± 0.3 and -8.61 ± 0.3)
442 (Fig. 4b). On the other hand, the deeper Alboran Sea provides a value of -9.8 ± 0.3 pointing to a



443 stronger contribution of WMDW (Jimenez-Espejo et al., 2015), coeval with the recovery of deep-water activity
444 from core MD99-2343 (Frigola et al., 2008).

445

446 **5.2 Hydrological changes in the Sardinia Channel during the Holocene**

447 The present-day hydrographic structure of the Sardinia Channel is characterized by four water masses, with the
448 surface, intermediate and deep-water masses being represented by MAW, LIW and TDW/WMDW, respectively
449 (Astraldi et al., 2002a; Millot and Taupier-Lepage, 2005). In addition, the WIW, flowing between the MAW and
450 the LIW, has also been observed along the Channel (Sammari et al., 1999). The core of the LIW is located at
451 400-450 m water depth in the Tyrrhenian Sea (Hopkins, 1988; Astraldi et al., 2002b), which is the depth range of
452 CWC samples from the Sardinia Channel (RECORD 23; 414 m) (Taviani et al., 2015). The youngest CWC
453 sample dated at ~0.1 ka BP has an ϵ_{Nd} value of -7.70 ± 0.10 (Table 1, Fig. 5), which is similar within error to the
454 value obtained from a seawater sample collected at 451 m close to the coral sampling location (-8.0 ± 0.4 ;
455 Montagna et al., in prep).

456 The CWC dating from the Sardinia Channel shows three distinct periods of sustained coral occurrence in this
457 area during the Holocene, with each displaying a large variability in ϵ_{Nd} values. CWC from the Early Holocene
458 (10.9-10.2 ka BP) and the Late Holocene (<1.5 ka BP) exhibit similar ranges of ϵ_{Nd} values (ranging from -5.99 ± 0.50 to
459 -7.75 ± 0.20 ; Table 1, Fig. 5c). Such variations are within the present-day ϵ_{Nd} range being
460 characteristic for intermediate waters in the eastern Mediterranean Sea (-6.6 ± 1.0 ; Tachikawa et al., 2004; Vance
461 et al., 2004). However, the CWC ϵ_{Nd} values are more radiogenic than those observed at mid-depth in the
462 present-day western basin (ranging from -10.4 ± 0.2 to -7.58 ± 0.47 ; Henry et al., 1994; Tachikawa et al., 2004;
463 Montagna et al., in prep), suggesting a stronger LIW component in the Sardinia Channel during the Early and
464 Late Holocene. The Sardinian CWC ϵ_{Nd} variability also reflects the sensitivity of the LIW to changes in the
465 eastern basin such as rapid variability of the Nile River flood discharge (Revel et al., 2014; 2015; Weldeab et al.,
466 2014) or a modification through time in the proportion between the LIW and the Cretan Intermediate Water
467 (CIW). Today, the intermediate water outflowing from the Strait of Sicily is composed by ~66 to 75 % of LIW
468 and 33 to 25 % of CIW (Manca et al., 2006; Millot, 2014). As the CIW is formed in the Aegean Sea, this
469 intermediate water mass is generally more radiogenic than LIW (Tachikawa et al., 2004; Montagna et al., in
470 prep). Following this hypothesis, a modification of the mixing proportion between the CIW and the LIW may
471 potentially explain values as radiogenic as about -6 in the Sardinia Channel during the Early and Late Holocene
472 (Fig. 5c). However, a stronger LIW and/or a CIW contribution cannot be responsible for ϵ_{Nd} values as low as
473 -8.66 ± 0.30 observed during the sapropel S1 event at 8.7 ka BP (Table 1, Fig. 5c). Considering that such
474 unradiogenic value is not observed at intermediate depth in the modern eastern Mediterranean basin, the most
475 plausible hypothesis suggested here is that the CWC were bathed in intermediate waters which were more
476 marked by the western basin.

477

478 **5.3 Hydrological implications for the intermediate water masses of the western Mediterranean Sea**

479 The ϵ_{Nd} records of the Balearic Sea, Alboran Sea and Sardinia Channel document a temporal variability of the
480 east-west gradient in the western Mediterranean basin during the Holocene. The magnitude of the gradient
481 ranges from ~1.5 to ~3 ϵ units during the Early and Late Holocene and it is strongly reduced at 8.7 ka BP,



482 coinciding with the sapropel S1 event affecting the eastern Mediterranean basin (Fig. 5). Such variations could
483 be the result of a modification of the Nd isotopic composition of intermediate water masses due to intensity
484 changes of the the LIW through time and a higher contribution of the western-sourced intermediate water
485 towards the Sardinia Channel coinciding with the sapropel S1 event.

486 The LIW acquires its radiogenic ϵ Nd in the Mediterranean Levantine basin mainly from Nd exchange between
487 seawater and lithogenic particles originating mainly from Nile River (Tachikawa et al., 2004). A higher sediment
488 supply from the Nile River starting at ~15 ka BP was documented by a shift to more radiogenic ϵ Nd values of
489 the terrigenous fraction obtained from a sediment core having been influenced by the Nile River discharge
490 (Revel et al., 2015) (Fig. 5e). However, others studies pointed to a gradual enhanced Nile River runoff as soon as
491 14.8 ka and a peak of Nile discharge from 9.7 to 8.4 ka recorded by large increase in sedimentation rate from 9.7
492 to 8.4 ka (>120 cm/ka) (Revel et al., 2015; Weldeab et al., 2014; Castaneda et al., 2016). The increase in Nile
493 River discharge has been related to the African Humid Period (14.8–5.5 ka BP; Shanahan et al., 2015), which in
494 turn was linked to the precessional increase in Northern Hemisphere insolation during low eccentricity
495 (deMenocal et al., 2000; Barker et al., 2004; Garcin et al., 2009). An increasing amount of radiogenic sediments
496 dominated by the Blue/Atbara Nile River contribution (Revel et al., 2014) could have modified the ϵ Nd of
497 surface water towards more radiogenic values (Revel et al., in prep). This signature was likely transferred to
498 intermediate depth as a consequence of the LIW formation in the Rhodes Gyre, and it might have been
499 propagated westwards towards the Sardinia Channel.

500 The Nile River runoff was also strongly enhanced during the sapropel S1 event (Revel et al., 2010; Weldeab et
501 al., 2014; Revel et al., 2014). Scrivner et al. (2004) have reported very high foraminifera ϵ Nd values (-3 to -3.5)
502 corresponding to the sapropel S1 event in the eastern Levantine Basin (ODP site 967; 34°04.27'N, 32°43.53'E;
503 2553 m water depth), pointing to a maximum Nile discharge at this time. Hence, considering the more
504 unradiogenic value of the CWC samples from the Sardinia Channel during the sapropel S1a event, it is very
505 unlikely that eastern-sourced water flowed at intermediate depth towards the Sardinia Channel. A possible
506 explanation could be the replacement of the radiogenic LIW that was no longer produced in the eastern basin
507 (Rohling, 1994) by less radiogenic western intermediate water (possibly WIW). Such a scenario could even
508 support previous hypotheses that invoke a potential circulation reversal in the eastern Mediterranean from anti-
509 estuarine to estuarine during sapropel formation (Huang and Stanley, 1972; Calvert, 1983; Sarmiento et al.,
510 1988; Buckley and Johnson, 1988; Thunell and Williams, 1989).

511

512 **6. Conclusions**

513 The foraminiferal ϵ Nd record from the intermediate Balearic Sea reveals a relatively narrow range of ϵ Nd values
514 varying between -9.50 and -8.61 since the LGM (~20 ka). Between 18 and 13.5 cal ka BP, the more
515 unradiogenic ϵ Nd values support a vigorous deep overturning in the Gulf of Lions while $\delta^{18}\text{O}$ and $\delta^{13}\text{C}$ values
516 indicate a stratification of the water masses after 16 cal ka BP. The stratification together with a decrease of the
517 deep-water intensity led to more radiogenic values after ~13 cal ka BP. The ϵ Nd record from planktonic
518 foraminifera, supplemented by CWC from the intermediate depths of the Alboran Sea, show only minor changes
519 in ϵ Nd values from 13.5 cal ka BP to 0.34 cal ka BP, suggesting that the westernmost part of the western
520 Mediterranean basin is not very sensitive to hydrological variations of the LIW.



521 On the contrary, CWC located at the depth of the LIW in the Sardinia Channel indicate high amplitude variations
522 of the ϵ_{Nd} values (between -7.75 ± 0.10 and -5.99 ± 0.50) during the Holocene, which could highlight either the
523 role of the Nile River in changing the ϵ_{Nd} of the LIW in the eastern Mediterranean basin or a different
524 LIW/CIW mixing of the water outflowing from the Strait of Sicily. Coinciding with the sapropel S1 event at
525 ~ 8.7 ka BP, CWC display a shift toward lower values (-8.66 ± 0.30), similar to those obtained at intermediate
526 depths in the westernmost part of the western basin. This suggests that western-sourced intermediate water likely
527 filled mid-depth of the southern Sardinia, replacing LIW that was no longer produced (or heavily reduced) in the
528 eastern basin. These results could potentially support a reversal of the Mediterranean circulation, although this
529 assumption needs further investigation to be confirmed.

530

531 Acknowledgements

532 The research leading to this study has received funding from the French National Research Agency
533 "Investissement d'Avenir" (n°ANR-10-LABX-0018), the HAMOC project ANR-13-BS06-0003, the
534 MISTRALS/PALEOMEX/COFIMED and ENVIMED/Boron Isotope and Trace Elements project. This work
535 contributes to the RITMARE project. We thank Hiske Fink for selecting and kindly providing the cold-water
536 corals samples from the Alboran Sea. We further thank François Thil and Louise Bordier for their support with
537 Nd isotopic composition analyses. Paolo Montagna is grateful for financial support from the Short Term
538 Mobility Program (CNR). Thanks are also extended to the captains, crews, chief scientists, and scientific parties
539 of research cruises RECORD (R/V Urania), POS-385 (R/V Poseidon) and PALEOCINAT II (R/V Le Suroît).

540

541 References

- 542 Abu-Zied, R. H., Rohling, E. J., Jorissen, F. J., Fontanier, C., Casford, J. S. L. and Cooke, S.: Benthic
543 foraminiferal response to changes in bottom-water oxygenation and organic carbon flux in the eastern
544 Mediterranean during LGM to Recent times, Mar. Micropaleontol., 67(1-2), 46–68,
545 doi:10.1016/j.marmicro.2007.08.006, 2008.
- 546 Allen, J. R. M., Huntley, B., Brandt, U., Brauer, A., Hubberten, H., Keller, J., Kraml, M., Mackensen, A.,
547 Mingram, J., Negendank, J. F. W., Nowaczyk, N. R., Oberhänsli, H., Watts, W. A., Wulf, S. and Zolitschka, B.:
548 Rapid environmental changes in southern Europe during the last glacial period, Nature, 400(6746), 740–743,
549 doi:10.1038/23432, 1999.
- 550 Andersen, M. B., Stirling, C. H., Zimmermann, B. and Halliday, A. N.: Precise determination of the open ocean
551 $^{234}\text{U}/^{238}\text{U}$ composition, Geochemistry, Geophys. Geosystems, 11(12), Q12003, doi:10.1029/2010GC003318,
552 2010.
- 553 Arsouze, T., Dutay, J.-C., Lacan, F. and Jeandel, C.: Reconstructing the Nd oceanic cycle using a coupled
554 dynamical – biogeochemical model, Biogeosciences, 6(12), 2829–2846, doi:10.5194/bg-6-2829-2009, 2009.
- 555 Astraldi, M., Gasparini, G. P., Gervasio, L. and Salusti, E.: Dense Water Dynamics along the Strait of Sicily
556 (Mediterranean Sea), J. Phys. Oceanogr., 31(12), 3457–3475, doi:10.1175/1520-
557 0485(2001)031<3457:DWDATS>2.0.CO;2, 2001.



- 558 Astraldi, M., Gasparini, G. P., Vetrano, A. and Vignudelli, S.: Hydrographic characteristics and interannual
559 variability of water masses in the central Mediterranean: A sensitivity test for long-term changes in the
560 Mediterranean Sea, Deep. Res. Part I Oceanogr. Res. Pap., 49(4), 661–680, doi:10.1016/S0967-0637(01)00059-
561 0, 2002a.
- 562 Astraldi, M., Conversano, F., Civitarese, G., Gasparini, G. P., Ribera d'Alcalà, M. and Vetrano, a.: Water mass
563 properties and chemical signatures in the central Mediterranean region, J. Mar. Syst., 33-34, 155–177,
564 doi:10.1016/S0924-7963(02)00057-X, 2002b.
- 565 Bahr, A., Kaboth, S., Jiménez-Espejo, F. J., Sierro, F. J., Voelker, A. H. L., Lourens, L., Röhl, U., Reichart, G.
566 J., Escutia, C., Hernández-Molina, F. J., Pross, J. and Friedrich, O.: Persistent monsoonal forcing of
567 Mediterranean Outflow Water dynamics during the late Pleistocene, Geology, 43(11), 951–954,
568 doi:10.1130/G37013.1, 2015.
- 569 Barker, P. A., Talbot, M. R., Street-Perrott, F. A., Marret, F., Scourse, J. and Odada, E. O.: Late Quaternary
570 climatic variability in intertropical Africa, in Past Climate Variability through Europe and Africa, pp. 117–138,
571 Springer Netherlands, Dordrecht., 2004.
- 572 Bartov, Y., Goldstein, S. L., Stein, M. and Enzel, Y.: Catastrophic arid episodes in the Eastern Mediterranean
573 linked with the North Atlantic Heinrich events, Geology, 31(5), 439, doi:10.1130/0091-
574 7613(2003)031<0439:CAEITE>2.0.CO;2, 2003.
- 575 Bigg, G. R. and Wadley, M. R.: Millennial-scale variability in the oceans: an ocean modelling view, J. Quat.
576 Sci., 16(4), 309–319, doi:10.1002/jqs.599, 2001.
- 577 Bout-Roumazeilles, V., Combourieu-Nebout, N., Desprat, S., Siani, G., Turon, J. L. and Essallami, L.: Tracking
578 atmospheric and riverine terrigenous supplies variability during the last glacial and the Holocene in central
579 Mediterranean, Clim. Past, 9(3), 1065–1087, doi:10.5194/cp-9-1065-2013, 2013.
- 580 Buckley, H. A. and Johnson, L. R.: Late pleistocene to recent sediment deposition in the central and western
581 Mediterranean, Deep Sea Res. Part A. Oceanogr. Res. Pap., 35(5), 749–766, doi:10.1016/0198-0149(88)90028-
582 3, 1988.
- 583 Cacho, I., Pelejero, C., Grimalt, J. O., Calafat, A. and Canals, M.: C37 alkenone measurements of sea surface
584 temperature in the Gulf of Lions (NW Mediterranean), Org. Geochem., 30(7), 557–566, doi:10.1016/S0146-
585 6380(99)00038-8, 1999.
- 586 Cacho, I., Grimalt, J. O., Sierro, F. J., Shackleton, N. and Canals, M.: Evidence for enhanced Mediterranean
587 thermohaline circulation during rapid climatic coolings, Earth Planet. Sci. Lett., 183(3-4), 417–429,
588 doi:10.1016/S0012-821X(00)00296-X, 2000.
- 589 Cacho, I., Grimalt, J. O., Canals, M., Sbaaffi, L., Shackleton, N. J., Schönfeld, J. and Zahn, R.: Variability of the
590 western Mediterranean Sea surface temperature during the last 25,000 years and its connection with the Northern
591 Hemisphere climatic changes, Paleoceanography, 16(1), 40–52, doi:10.1029/2000PA000502, 2001.



- 592 Cacho, I., Grimalt, J. O. and Canals, M.: Response of the Western Mediterranean Sea to rapid climatic variability
593 during the last 50,000 years: a molecular biomarker approach, *J. Mar. Syst.*, 33-34, 253–272,
594 doi:10.1016/S0924-7963(02)00061-1, 2002.
- 595 Cacho, I., Shackleton, N., Elderfield, H., Sierro, F. J. and Grimalt, J. O.: Glacial rapid variability in deep-water
596 temperature and $\delta^{18}\text{O}$ from the Western Mediterranean Sea, *Quat. Sci. Rev.*, 25(23-24), 3294–3311,
597 doi:10.1016/j.quascirev.2006.10.004, 2006.
- 598 Calvert, S. E.: Geochemistry of Pleistocene sapropels and associated sediments from the Eastern Mediterranean,
599 *Oceanol. Acta*, 6(3), 255–267, 1983.
- 600 Castañeda, I. S., Schouten, S., Pätzold, J., Lucassen, F., Kasemann, S., Kuhlmann, H. and Schefuß, E.:
601 Hydroclimate variability in the Nile River Basin during the past 28,000 years, *Earth Planet. Sci. Lett.*, 438, 47–
602 56, doi:10.1016/j.epsl.2015.12.014, 2016.
- 603 Cheng, H., Lawrence Edwards, R., Shen, C.-C., Polyak, V. J., Asmerom, Y., Woodhead, J. D., Hellstrom, J.,
604 Wang, Y., Kong, X., Spötl, C., Wang, X. and Calvin Alexander, E.: Improvements in ^{230}Th dating, ^{230}Th and
605 ^{234}U half-life values, and U-Th isotopic measurements by multi-collector inductively coupled plasma mass
606 spectrometry, *Earth Planet. Sci. Lett.*, 371-372, 82–91, doi:10.1016/j.epsl.2013.04.006, 2013.
- 607 Colin, C., Frank, N., Copard, K. and Douville, E.: Neodymium isotopic composition of deep-sea corals from the
608 NE Atlantic: implications for past hydrological changes during the Holocene, *Quat. Sci. Rev.*, 29(19-20), 2509–
609 2517, doi:10.1016/j.quascirev.2010.05.012, 2010.
- 610 Combourieu-Nebout, N., Turon, J. L., Zahn, R., Capotondi, L., Londeix, L. and Pahnke, K.: Enhanced aridity
611 and atmospheric high-pressure stability over the western Mediterranean during the North Atlantic cold events of
612 the past 50 k.y., *Geology*, 30(10), 863–866, doi:10.1130/0091-7613(2002)030<0863:EAAAHP>2.0.CO;2, 2002.
- 613 Copard, K., Colin, C., Douville, E., Freiwald, A., Gudmundsson, G., De Mol, B. and Frank, N.: Nd isotopes in
614 deep-sea corals in the North-eastern Atlantic, *Quat. Sci. Rev.*, 29(19-20), 2499–2508,
615 doi:10.1016/j.quascirev.2010.05.025, 2010.
- 616 Copard, K., Colin, C., Henderson, G. M., Scholten, J., Douville, E., Sicre, M.-A. and Frank, N.: Late Holocene
617 intermediate water variability in the northeastern Atlantic as recorded by deep-sea corals, *Earth Planet. Sci. Lett.*,
618 313-314, 34–44, doi:10.1016/j.epsl.2011.09.047, 2012.
- 619 Cramp, A. and O'Sullivan, G.: Neogene sapropels in the Mediterranean: a review, *Mar. Geol.*, 153(1-4), 11–28,
620 doi:10.1016/S0025-3227(98)00092-9, 1999.
- 621 DeMenocal, P., Ortiz, J., Guilderson, T. and Sarnthein, M.: Coherent High- and Low-Latitude Climate
622 Variability During the Holocene Warm Period, *Science* (80-. .), 288(5474), 2198–2202,
623 doi:10.1126/science.288.5474.2198, 2000.
- 624 Deschamps, P., Durand, N., Bard, E., Hamelin, B., Camoin, G., Thomas, A. L., Henderson, G. M., Okuno, J. and
625 Yokoyama, Y.: Ice-sheet collapse and sea-level rise at the Bølling warming 14,600 years ago, *Nature*,



- 626 483(7391), 559–564, doi:10.1038/nature10902, 2012.
- 627 Douville, E., Sallé, E., Frank, N., Eisele, M., Pons-Branchu, E. and Ayral, S.: Rapid and accurate U–Th dating
628 of ancient carbonates using inductively coupled plasma-quadrupole mass spectrometry, *Chem. Geol.*, 272(1–4),
629 1–11, doi:10.1016/j.chemgeo.2010.01.007, 2010.
- 630 Dubois-Dauphin, Q., Colin, C., Bonneau, L., Montagna, P., Wu, Q., Van Rooij, D., Reverdin, G., Douville, E.,
631 Thil, F., Waldner, A., Frank, N.: Fingerprinting North-east Atlantic water masses using Neodymium isotopes,
632 EPSL, Submitted.
- 633
- 634 Elmore, A. C., Piotrowski, A. M., Wright, J. D. and Scrivner, A. E.: Testing the extraction of past seawater Nd
635 isotopic composition from North Atlantic deep sea sediments and foraminifera, *Geochemistry, Geophys.
636 Geosystems*, 12(9), doi:10.1029/2011GC003741, 2011.
- 637 Emeis, K.-C., Sakamoto, T., Wehausen, R. and Brumsack, H.-J.: The sapropel record of the eastern
638 Mediterranean Sea — results of Ocean Drilling Program Leg 160, *Palaeogeogr. Palaeoclimatol. Palaeoecol.*,
639 158(3–4), 371–395, doi:10.1016/S0031-0182(00)00059-6, 2000.
- 640 Fink, H. G., Wienberg, C., De Pol-Holz, R., Wintersteller, P. and Hebbeln, D.: Cold-water coral growth in the
641 Alboran Sea related to high productivity during the Late Pleistocene and Holocene, *Mar. Geol.*, 339, 71–82,
642 doi:10.1016/j.margeo.2013.04.009, 2013.
- 643 Frigola, J., Moreno, A., Cacho, I., Canals, M., Sierro, F. J., Flores, J. a., Grimalt, J. O., Hodell, D. a. and Curtis,
644 J. H.: Holocene climate variability in the western Mediterranean region from a deepwater sediment record,
645 *Paleoceanography*, 22(2), n/a–n/a, doi:10.1029/2006PA001307, 2007.
- 646 Frigola, J., Moreno, A., Cacho, I., Canals, M., Sierro, F. J., Flores, J. A. and Grimalt, J. O.: Evidence of abrupt
647 changes in Western Mediterranean Deep Water circulation during the last 50kyr: A high-resolution marine
648 record from the Balearic Sea, *Quat. Int.*, 181(1), 88–104, doi:10.1016/j.quaint.2007.06.016, 2008.
- 649 Garcin, Y., Junginger, A., Melnick, D., Olago, D. O., Strecker, M. R. and Trauth, M. H.: Late Pleistocene–
650 Holocene rise and collapse of Lake Suguta, northern Kenya Rift, *Quat. Sci. Rev.*, 28(9–10), 911–925,
651 doi:10.1016/j.quascirev.2008.12.006, 2009.
- 652 Grousset, F. E. and Biscaye, P. E.: Tracing dust sources and transport patterns using Sr, Nd and Pb isotopes,
653 *Chem. Geol.*, 222(3–4), 149–167, doi:10.1016/j.chemgeo.2005.05.006, 2005.
- 654 Grousset, F. E., Rognon, P., Coudé-Gaussen, G. and Pédehay, P.: Origins of peri-Saharan dust deposits traced
655 by their Nd and Sr isotopic composition, *Palaeogeogr. Palaeoclimatol. Palaeoecol.*, 93(3–4), 203–212,
656 doi:10.1016/0031-0182(92)90097-O, 1992.
- 657 Grousset, F. E., Parra, M., Bory, A., Martinez, P., Bertrand, P., Shimmield, G. and Ellam, R. M.: Saharan wind
658 regimes traced by the Sr-Nd isotopic composition of subtropical Atlantic sediments: Last Glacial Maximum vs
659 today, *Quat. Sci. Rev.*, 17, 395–409, doi:10.1016/S0277-3791(97)00048-6, 1998.



- 660 Hebbeln, D., Wienberg, C., Beuck, L., Freiwald, A., Wintersteller, P. and cruise participants (2009) Report and
661 preliminary results of R/V POSEIDON Cruise 385 "Cold-water corals of the Alboran Sea (western
662 Mediterranean Sea)", Faro - Toulon, 29.5. - 16.6.2009. Reports of the Department of Geosciences at the
663 University of Bremen, No. 273. Department of Geosciences, Bremen University. urn:nbn:de:gbv:46-
664 ep000106508.
- 665 Henry, F., Jeandel, C., Dupré, B. and Minster, J.-F.: Particulate and dissolved Nd in the western Mediterranean
666 Sea: Sources, fate and budget, Mar. Chem., 45(4), 283–305, doi:10.1016/0304-4203(94)90075-2, 1994.
- 667 Hooghiemstra, H., Bechler, A. and Beug, H.-J.: Isopollen maps for 18,000 years B.P. of the Atlantic offshore of
668 northwest Africa: Evidence for paleowind circulation, Paleoceanography, 2, 561–582,
669 doi:10.1029/PA002i006p00561, 1987.
- 670 Hopkins, T. S.: Recent observations on the intermediate and deep water circulation in the Southern Tyrrhenian
671 Sea, Oceanol. Acta, (Special issue), 41–50, 1988.
- 672 Huang, T. C. and Stanley, D. J.: Western Alboran sea: sediment dispersal, pounding and reversal of currents, in
673 The Mediterranean Sea: A Natural Sedimentation Laboratory, pp. 521–559, Dowden, Hutchinson & Ross,
674 Stroudsburg, PA., 1972.
- 675 Hutson, W. H.: The Agulhas Current During the Late Pleistocene: Analysis of Modern Faunal Analogs, Science
676 (80-.), 207(4426), 64–66, doi:10.1126/science.207.4426.64, 1980.
- 677 Itambi, a. C., von Dobeneck, T., Mulitza, S., Bickert, T. and Heslop, D.: Millennial-scale northwest African
678 droughts related to Heinrich events and Dansgaard-Oeschger cycles: Evidence in marine sediments from
679 offshore Senegal, Paleoceanography, 24(1), PA1205, doi:10.1029/2007PA001570, 2009.
- 680 Ivy-Ochs, S., Kerschner, H. and Schlüchter, C.: Cosmogenic nuclides and the dating of Lateglacial and Early
681 Holocene glacier variations: The Alpine perspective, Quat. Int., 164-165, 53–63,
682 doi:10.1016/j.quaint.2006.12.008, 2007.
- 683 Jacobsen, S. B. and Wasserburg, G. J.: Sm-Nd isotopic evolution of chondrites, Earth Planet. Sci. Lett., 50(1),
684 139–155, doi:10.1016/0012-821X(80)90125-9, 1980.
- 685 Jaffey, A. H., Flynn, K. F., Glendenin, L. E., Bentley, W. C. and Essling, A. M.: Precision measurements of half-
686 lives and specific activities of ^{235}U and ^{238}U , Phys. Rev. C, 4(5), 1889–1906, doi:10.1103/PhysRevC.4.1889,
687 1971.
- 688 Jiménez-Espejo, F. J., Pardos-Gené, M., Martínez-Ruiz, F., García-Alix, A., van de Flierdt, T., Toyofuku, T.,
689 Bahr, A. and Kreissig, K.: Geochemical evidence for intermediate water circulation in the westernmost
690 Mediterranean over the last 20kyrBP and its impact on the Mediterranean Outflow, Glob. Planet. Change, 135,
691 38–46, doi:10.1016/j.gloplacha.2015.10.001, 2015.
- 692 Kallel, N., Paterne, M., Labeyrie, L., Duplessy, J.-C. and Arnold, M.: Temperature and salinity records of the
693 Tyrrhenian Sea during the last 18,000 years, Palaeogeogr. Palaeoclimatol. Palaeoecol., 135(1-4), 97–108,



- 694 doi:10.1016/S0031-0182(97)00021-7, 1997.
- 695 Kelly, M. A., Ivy-Ochs, S., Kubik, P. W., Von Blanckenburg, F. and Schlüchter, C.: Chronology of deglaciation
696 based on ^{10}Be dates of glacial erosional features in the Grimsel Pass region, central Swiss Alps, *Boreas*, 35(4),
697 634–643, doi:10.1111/j.1502-3885.2006.tb01169.x, 2006.
- 698 Khelifi, N., Sarnthein, M., Andersen, N., Blanz, T., Frank, M., Garbe-Schonberg, D., Haley, B. a., Stumpf, R.
699 and Weinelt, M.: A major and long-term Pliocene intensification of the Mediterranean outflow, 3.5–3.3 Ma ago,
700 *Geology*, 37(9), 811–814, doi:10.1130/G30058A.1, 2009.
- 701 Kinder, T. H. and Parrilla, G.: Yes, some of the Mediterranean water does come from great depth, *J. Geophys.
702 Res.*, 92, 2901–2906, doi:10.1029/JC092iC03p02901, 1987.
- 703 Kuhnt, T., Schmiedl, G., Ehrmann, W., Hamann, Y. and Hemleben, C.: Deep-sea ecosystem variability of the
704 Aegean Sea during the past 22 kyr as revealed by Benthic Foraminifera, *Mar. Micropaleontol.*, 64(3-4), 141–
705 162, doi:10.1016/j.marmicro.2007.04.003, 2007.
- 706 Kuhnt, T., Schmiedl, G., Ehrmann, W., Hamann, Y. and Andersen, N.: Stable isotopic composition of Holocene
707 benthic foraminifers from the Eastern Mediterranean Sea: Past changes in productivity and deep water
708 oxygenation, *Palaeogeogr. Palaeoclimatol. Palaeoecol.*, 268(1-2), 106–115, doi:10.1016/j.palaeo.2008.07.010,
709 2008.
- 710 Lacan, F. and Jeandel, C.: Tracing Papua New Guinea imprint on the central Equatorial Pacific Ocean using
711 neodymium isotopic compositions and Rare Earth Element patterns, *Earth Planet. Sci. Lett.*, 186(3-4), 497–512,
712 doi:10.1016/S0012-821X(01)00263-1, 2001.
- 713 Lacan, F. and Jeandel, C.: Neodymium isotopes as a new tool for quantifying exchange fluxes at the continent–
714 ocean interface, *Earth Planet. Sci. Lett.*, 232(3-4), 245–257, doi:10.1016/j.epsl.2005.01.004, 2005.
- 715 Lascaratos, A. and Nittis, K.: A high-resolution three-dimensional numerical study of intermediate water
716 formation in the Levantine Sea, *J. Geophys. Res.*, 103(C9), 18497, doi:10.1029/98JC01196, 1998.
- 717 Lascaratos, A., Williams, R. G. and Tragou, E.: A mixed-layer study of the formation of Levantine intermediate
718 water, *J. Geophys. Res.*, 98(C8), 14739, doi:10.1029/93JC00912, 1993.
- 719 López Correa, M., Montagna, P., Joseph, N., Rüggeberg, A., Fietzke, J., Flögel, S., Dorschel, B., Goldstein, S.
720 L., Wheeler, A. and Freiwald, A.: Preboreal onset of cold-water coral growth beyond the Arctic Circle revealed
721 by coupled radiocarbon and U-series dating and neodymium isotopes, *Quat. Sci. Rev.*, 34, 24–43,
722 doi:10.1016/j.quascirev.2011.12.005, 2012.
- 723 López-Jurado, J. L., Marcos, M. and Monserrat, S.: Hydrographic conditions affecting two fishing grounds of
724 Mallorca island (Western Mediterranean): during the IDEA Project (2003–2004), *J. Mar. Syst.*, 71(3-4), 303–
725 315, doi:10.1016/j.jmarsys.2007.03.007, 2008.
- 726 Ludwig, K. R. and Titterington, D. M.: Calculation of $^{230}\text{Th}/\text{U}$ isochrons, ages, and errors, *Geochim.*



- 727 Cosmochim. Acta, 58(22), 5031–5042, doi:[http://dx.doi.org/10.1016/0016-7037\(94\)90229-1](http://dx.doi.org/10.1016/0016-7037(94)90229-1), 1994.
- 728 Lugmair, G. W., Shimamura, T., Lewis, R. S. and Anders, E.: Samarium-146 in the Early Solar System:
729 Evidence from Neodymium in the Allende Meteorite, Science (80- .), 222(4627), 1015–1018,
730 doi:[10.1126/science.222.4627.1015](https://doi.org/10.1126/science.222.4627.1015), 1983.
- 731 Malanotte-Rizzoli, P., Manca, B. B., D'Alcala, M. R., Theocharis, A., Brenner, S., Budillon, G. and Ozsoy, E.:
732 The Eastern Mediterranean in the 80s and in the 90s: the big transition in the intermediate and deep circulations,
733 Dyn. Atmos. Ocean., 29(2-4), 365–395, doi:[10.1016/S0377-0265\(99\)00011-1](https://doi.org/10.1016/S0377-0265(99)00011-1), 1999.
- 734 Manca, B., Ibello, V., Pacciaroni, M., Scarazzato, P. and Giorgetti, A.: Ventilation of deep waters in the Adriatic
735 and Ionian Seas following changes in thermohaline circulation of the Eastern Mediterranean, Clim. Res., 31,
736 239–256, doi:[10.3354/cr031239](https://doi.org/10.3354/cr031239), 2006.
- 737 Martrat, B., Grimalt, J. O., Lopez-Martinez, C., Cacho, I., Sierro, F. J., Flores, J. A., Zahn, R., Canals, M.,
738 Curtis, J. H. and Hodell, D. a: Abrupt temperature changes in the Western Mediterranean over the past 250,000
739 years., Science (80- .), 306(5702), 1762–1765, doi:[10.1126/science.1101706](https://doi.org/10.1126/science.1101706), 2004.
- 740 Melki, T., Kallel, N., Jorissen, F. J., Guichard, F., Dennielou, B., Berné, S., Labeyrie, L. and Fontugne, M.:
741 Abrupt climate change, sea surface salinity and paleoproductivity in the western Mediterranean Sea (Gulf of
742 Lion) during the last 28 kyr, Palaeogeogr. Palaeoclimatol. Palaeoecol., 279(1-2), 96–113,
743 doi:[10.1016/j.palaeo.2009.05.005](https://doi.org/10.1016/j.palaeo.2009.05.005), 2009.
- 744
- 745 Mercone, D., Thomson, J., Croudace, I. W., Siani, G., Paterne, M. and Troelstra, S.: Duration of S1, the most
746 recent sapropel in the eastern Mediterranean Sea, as indicated by accelerator mass spectrometry radiocarbon and
747 geochemical evidence, Paleoceanography, 15(3), 336–347, doi:[10.1029/1999PA000397](https://doi.org/10.1029/1999PA000397), 2000.
- 748 Mercone, D., Thomson, J., Abu-Zied, R. H., Croudace, I. W. and Rohling, E. J.: High-resolution geochemical
749 and micropalaeontological profiling of the most recent eastern Mediterranean sapropel, Mar. Geol., 177(1-2),
750 25–44, doi:[10.1016/S0025-3227\(01\)00122-0](https://doi.org/10.1016/S0025-3227(01)00122-0), 2001.
- 751 Millot, C.: Circulation in the Western Mediterranean Sea, J. Mar. Syst., 20(1-4), 423–442, doi:[10.1016/S0924-7963\(98\)00078-5](https://doi.org/10.1016/S0924-7963(98)00078-5), 1999.
- 753 Millot, C.: Another description of the Mediterranean Sea outflow, Prog. Oceanogr., 82(2), 101–124,
754 doi:[10.1016/j.pocean.2009.04.016](https://doi.org/10.1016/j.pocean.2009.04.016), 2009.
- 755 Millot, C.: Heterogeneities of in- and out-flows in the Mediterranean Sea, Prog. Oceanogr., 120, 254–278,
756 doi:[10.1016/j.pocean.2013.09.007](https://doi.org/10.1016/j.pocean.2013.09.007), 2014.
- 757 Millot, C. and Taupier-Letage, I.: Circulation in the Mediterranean Sea, in Environmental Chemistry, vol. 5,
758 edited by A. Saliot, pp. 29–66, Springer Berlin Heidelberg, Heidelberg., 2005.
- 759 Millot, C., Candela, J., Fuda, J.-L. and Tber, Y.: Large warming and salinification of the Mediterranean outflow
760 due to changes in its composition, Deep Sea Res. Part I Oceanogr. Res. Pap., 53(4), 656–666,



- 761 doi:10.1016/j.dsr.2005.12.017, 2006.
- 762 Montero-Serrano, J.-C., Frank, N., Colin, C., Wienberg, C. and Eisele, M.: The climate influence on the mid-
763 depth Northeast Atlantic gyres viewed by cold-water corals, *Geophys. Res. Lett.*, 38(19),
764 doi:10.1029/2011GL048733, 2011.
- 765 Montero-Serrano, J.-C., Frank, N., Tisnérat-Laborde, N., Colin, C., Wu, C., Lin, K., Shen, C., Copard, K.,
766 Orejas, C., Gori, A., De Mol, L., Van Rooij, D., Reverdin, G. and Douville, E.: Decadal changes in the mid-
767 depth water mass dynamic of the Northeastern Atlantic margin (Bay of Biscay), *Earth Planet. Sci. Lett.*, 364,
768 134–144, doi:10.1016/j.epsl.2013.01.012, 2013.
- 769 Moreno, A., Cacho, I., Canals, M., Prins, M. a., Sánchez-Goñi, M.-F., Grimal, O. J. and Weltje, G. J.: Saharan
770 Dust Transport and High-Latitude Glacial Climatic Variability: The Alboran Sea Record, *Quat. Res.*, 58, 318–
771 328, doi:10.1006/qres.2002.2383, 2002.
- 772 Moreno, A., Cacho, I., Canals, M., Grimalt, J. O., Sánchez-Goñi, M. F., Shackleton, N. and Sierro, F. J.: Links
773 between marine and atmospheric processes oscillating on a millennial time-scale. A multi-proxy study of the last
774 50,000yr from the Alboran Sea (Western Mediterranean Sea), *Quat. Sci. Rev.*, 24(14-15), 1623–1636,
775 doi:10.1016/j.quascirev.2004.06.018, 2005.
- 776 Ovchinnikov, I. M.: The formation of intermediate water in the Mediterranean, *Oceanology*, 24, 168–173, 1984.
- 777 Overpeck, J. T., Webb, T. and Prentice, I. C.: Quantitative interpretation of fossil pollen spectra: Dissimilarity
778 coefficients and the method of modern analogs, *Quat. Res.*, 23(1), 87–108, doi:10.1016/0033-5894(85)90074-2,
779 1985.
- 780 Patrén, M., Kallel, N., Labeyrie, L., Vautravers, M., Duplessy, J.-C., Rossignol-Strick, M., Cortijo, E., Arnold,
781 M. and Fontugne, M.: Hydrological relationship between the North Atlantic Ocean and the Mediterranean Sea
782 during the past 15-75 kyr, *Paleoceanography*, 14(5), 626–638, doi:10.1029/1998PA900022, 1999.
- 783 Pérez-Folgado, M., Sierro, F. J., Flores, J. A., Cacho, I., Grimalt, J. O., Zahn, R. and Shackleton, N.: Western
784 Mediterranean planktonic foraminifera events and millennial climatic variability during the last 70 kyr, *Mar.
785 Micropaleontol.*, 48(1-2), 49–70, doi:10.1016/S0377-8398(02)00160-3, 2003.
- 786 Pinardi, N. and Masetti, E.: Variability of the large scale general circulation of the Mediterranean Sea from
787 observations and modelling: a review, *Palaeogeogr. Palaeoclimatol. Palaeoecol.*, 158(3-4), 153–173,
788 doi:10.1016/S0031-0182(00)00048-1, 2000.
- 789 Piotrowski, A. M., Galy, A., Nicholl, J. a. L., Roberts, N. L., Wilson, D. J., Clegg, J. a. and Yu, J.:
790 Reconstructing deglacial North and South Atlantic deep water sourcing using foraminiferal Nd isotopes, *Earth
791 Planet. Sci. Lett.*, 357-358, 289–297, doi:10.1016/j.epsl.2012.09.036, 2012.
- 792 Pons-Branchu, E., Douville, E., Roy-Barman, M., Dumont, E., Branchu, P., Thil, F., Frank, N., Bordier, L. and
793 Borst, W.: A geochemical perspective on Parisian urban history based on U-Th dating, laminae counting and
794 yttrium and REE concentrations of recent carbonates in underground aqueducts, *Quat. Geochronol.*, 24, 44–53,



- 795 doi:10.1016/j.quageo.2014.08.001, 2014.
- 796 Prell, W. L.: Stability of low-latitude sea-surface temperatures: an evaluation of the CLIMAP reconstruction
797 with emphasis on the positive SST anomalies. Final report, Providence, RI (USA)., 1985.
- 798 Reimer, P. J., Bard, E., Bayliss, A., Beck, J. W., Blackwell, P. G., Bronk Ramsey, C., Grootes, P. M.,
799 Guilderson, T. P., Haflidason, H., Hajdas, I., HattŽ, C., Heaton, T. J., Hoffmann, D. L., Hogg, A. G., Hughen, K.
800 A., Kaiser, K. F., Kromer, B., Manning, S. W., Niu, M., Reimer, R. W., Richards, D. A., Scott, E. M., Southon,
801 J. R., Staff, R. A., Turney, C. S. M., & van der Plicht, J. (2013). IntCal13 and Marine13 Radiocarbon Age
802 Calibration Curves 0-50,000 Years cal BP. *Radiocarbon*, 55(4).
- 803 Revel, M., Ducassou, E., Grousset, F. E., Bernasconi, S., Migeon, S., Revillon, S., Mascle, J., Murat, A.,
804 Zaragosi, S. and Bosch, D.: 100,000 Years of African monsoon variability recorded in sediments of the Nile
805 margin, *Quat. Sci. Rev.*, 29(11-12), 1342–1362, doi:10.1016/j.quascirev.2010.02.006, 2010.
- 806 Revel, M., Colin, C., Bernasconi, S., Combourieu-Nebout, N., Ducassou, E., Grousset, F. E., Rolland, Y.,
807 Migeon, S., Bosch, D., Brunet, P., Zhao, Y. and Mascle, J.: 21,000 Years of Ethiopian African monsoon
808 variability recorded in sediments of the western Nile deep-sea fan, *Reg. Environ. Chang.*, 14(5), 1685–1696,
809 doi:10.1007/s10113-014-0588-x, 2014.
- 810 Revel, M., Ducassou, E., Skonieczny, C., Colin, C., Bastian, L., Bosch, D., Migeon, S. and Mascle, J.: 20,000
811 years of Nile River dynamics and environmental changes in the Nile catchment area as inferred from Nile upper
812 continental slope sediments, *Quat. Sci. Rev.*, 130, 200–221, doi:10.1016/j.quascirev.2015.10.030, 2015.
- 813 Roberts, N. L., Piotrowski, A. M., McManus, J. F. and Keigwin, L. D.: Synchronous deglacial overturning and
814 water mass source changes., *Science*, 327(2010), 75–78, doi:10.1126/science.1178068, 2010.
- 815 Rogerson, M., Rohling, E. J., Weaver, P. P. E. and Murray, J. W.: Glacial to interglacial changes in the settling
816 depth of the Mediterranean Outflow plume, *Paleoceanography*, 20(3), doi:10.1029/2004PA001106, 2005.
- 817 Rogerson, M., Rohling, E. J. and Weaver, P. P. E.: Promotion of meridional overturning by Mediterranean-
818 derived salt during the last deglaciation, *Paleoceanography*, 21(4), 1–8, doi:10.1029/2006PA001306, 2006.
- 819 Rogerson, M., Cacho, I., Jimenez-Espejo, F., Reguera, M. I., Sierro, F. J., Martinez-Ruiz, F., Frigola, J. and
820 Canals, M.: A dynamic explanation for the origin of the western Mediterranean organic-rich layers,
821 *Geochemistry, Geophys. Geosystems*, 9(7), n/a–n/a, doi:10.1029/2007GC001936, 2008.
- 822 Rohling, E. J.: Review and new aspects concerning the formation of eastern Mediterranean sapropels, *Mar.
823 Geol.*, 122(1-2), 1–28, doi:10.1016/0025-3227(94)90202-X, 1994.
- 824 Rohling, E. J., Jorissen, F. J. and De stigter, H. C.: 200 Year interruption of Holocene sapropel formation in the
825 Adriatic Sea, *J. Micropalaeontology*, 16(2), 97–108, doi:10.1144/jm.16.2.97, 1997.
- 826 Rohling, E. J., Mayewski, P. a., Abu-Zied, R. H., Casford, J. S. L. and Hayes, A.: Holocene atmosphere-ocean
827 interactions: records from Greenland and the Aegean Sea, *Clim. Dyn.*, 18(7), 587–593, doi:10.1007/s00382-001-



- 828 0194-8, 2002.
- 829 Rohling, E. J., Sprovieri, M., Cane, T., Casford, J. S. , Cooke, S., Bouloubassi, I., Emeis, K. C., Schiebel, R.,
830 Rogerson, M., Hayes, A., Jorissen, F. . and Kroon, D.: Reconstructing past planktic foraminiferal habitats using
831 stable isotope data: a case history for Mediterranean sapropel S5, *Mar. Micropaleontol.*, 50(1-2), 89–123,
832 doi:10.1016/S0377-8398(03)00068-9, 2004.
- 833 Rohling, E. J., Marino, G. and Grant, K. M.: Mediterranean climate and oceanography, and the periodic
834 development of anoxic events (sapropels), *Earth-Science Rev.*, 143, 62–97, doi:10.1016/j.earscirev.2015.01.008,
835 2015.
- 836 Rossignol-Strick, M., Nesteroff, W., Olive, P. and Vergnaud-Grazzini, C.: After the deluge: Mediterranean
837 stagnation and sapropel formation, *Nature*, 295(5845), 105–110, doi:10.1038/295105a0, 1982.
- 838 Sammari, C., Millot, C., Taupier-Letage, I., Stefani, A. and Brahim, M.: Hydrological characteristics in the
839 Tunisia–Sardinia–Sicily area during spring 1995, *Deep Sea Res. Part I Oceanogr. Res. Pap.*, 46(10), 1671–1703,
840 doi:10.1016/S0967-0637(99)00026-6, 1999.
- 841 Sarmiento, J. L., Herbert, T. and Toggweiler, J. R.: Mediterranean nutrient balance and episodes of anoxia,
842 *Global Biogeochem. Cycles*, 2(4), 427–444, doi:10.1029/GB002i004p00427, 1988.
- 843
- 844 Sánchez-Góñi, M., Cacho, I., Turon, J. L., Guiot, J., Sierra, F. J., Peypouquet, J., Grimalt, J. O. and Shackleton,
845 N. J.: Synchronicity between marine and terrestrial responses to millennial scale climatic variability during the
846 last glacial period in the Mediterranean region, *Clim. Dyn.*, 19(1), 95–105, doi:10.1007/s00382-001-0212-x,
847 2002.
- 848 Sarnthein, M., Tetzlaff, G., Koopmann, B., Wolter, K. and Pflaumann, U.: Glacial and interglacial wind regimes
849 over the eastern subtropical Atlantic and North-West Africa, *Nature*, 293, 193–196, doi:10.1038/293193a0,
850 1981.
- 851 Schmiedl, G., Kuhnt, T., Ehrmann, W., Emeis, K. C., Hamann, Y., Kotthoff, U., Dulski, P. and Pross, J.:
852 Climatic forcing of eastern Mediterranean deep-water formation and benthic ecosystems during the past 22 000
853 years, *Quat. Sci. Rev.*, 29(23-24), 3006–3020, doi:10.1016/j.quascirev.2010.07.002, 2010.
- 854 Schönfeld, J. and Zahn, R.: Late Glacial to Holocene history of the Mediterranean outflow. Evidence from
855 benthic foraminiferal assemblages and stable isotopes at the Portuguese margin, *Palaeogeogr. Palaeoclimatol.*
856 *Palaeoecol.*, 159(1-2), 85–111, doi:10.1016/S0031-0182(00)00035-3, 2000.
- 857 Schott, F., Visbeck, M., Send, U., Fischer, J., Stramma, L. and Desaubies, Y.: Observations of Deep Convection
858 in the Gulf of Lions, Northern Mediterranean, during the Winter of 1991/92, *J. Phys. Oceanogr.*, 26(4), 505–524,
859 doi:10.1175/1520-0485(1996)026<0505:OOCIT>2.0.CO;2, 1996.
- 860 Schroeder, K., Millot, C., Bengara, L., Ben Ismail, S., Bensi, M., Borghini, M., Budillon, G., Cardin, V.,
861 Coppola, L., Curtill, C., Drago, A., El Moumni, B., Font, J., Fuda, J. L., García-Lafuente, J., Gasparini, G. P.,
862 Kontoyiannis, H., Lefevre, D., Puig, P., Raimbault, P., Rougier, G., Salat, J., Sammari, C., Sánchez Garrido, J.



- 863 C., Sanchez-Roman, A., Sarnocchia, S., Tamburini, C., Taupier-Letage, I., Theocharis, A., Vargas-Yáñez, M.
864 and Vetrano, A.: Long-term monitoring programme of the hydrological variability in the Mediterranean Sea: a
865 first overview of the HYDROCHANGES network, *Ocean Sci.*, 9(2), 301–324, doi:10.5194/os-9-301-2013,
866 2013.
- 867 Scrivner, A. E., Vance, D. and Rohling, E. J.: New neodymium isotope data quantify Nile involvement in
868 Mediterranean anoxic episodes, *Geology*, 32(7), 565, doi:10.1130/G20419.1, 2004.
- 869 Shanahan, T. M., McKay, N. P., Hughen, K. A., Overpeck, J. T., Otto-Bliesner, B., Heil, C. W., King, J., Scholz,
870 C. A. and Peck, J.: The time-transgressive termination of the African Humid Period, *Nat. Geosci.*, 8(2), 140–144,
871 doi:10.1038/ngeo2329, 2015.
- 872 Siani, G., Paterne, M., Arnold, M., Bard, E., Metivier, B., Tisnerat, N. and Bassinot, F.: Radiocarbon reservoir
873 ages in the Mediterranean Sea and Black Sea, *Radiocarbon*, 42(2), 271–280 [online] Available from: <Go to
874 ISI>://000089971000010, 2000.
- 875 Siani, G., Paterne, M., Michel, E., Sulpizio, R., Sbrana, A., Arnold, M. and Haddad, G.: Mediterranean Sea
876 surface radiocarbon reservoir age changes since the last glacial maximum., *Science* (80-.), 294(5548), 1917–
877 1920, doi:10.1126/science.1063649, 2001.
- 878 Siani, G., Sulpizio, R., Paterne, M. and Sbrana, A.: Tephrostratigraphy study for the last 18,000 C years in a
879 deep-sea sediment sequence for the South Adriatic, *Quat. Sci. Rev.*, 23(23-24), 2485–2500,
880 doi:10.1016/j.quascirev.2004.06.004, 2004.
- 881 Siani, G., Magny, M., Paterne, M., Debret, M., Fontugne, M. (2013) - Paleohydrology reconstruction and
882 Holocene climate variability in the South Adriatic Sea. *Climate of the Past*, 9, 499–515.
- 883 Sierra, F. J., Hodell, D. A., Curtis, J. H., Flores, J. A., Reguera, I., Colmenero-Hidalgo, E., Bárcena, M. A.,
884 Grimalt, J. O., Cacho, I., Frigola, J. and Canals, M.: Impact of iceberg melting on Mediterranean thermohaline
885 circulation during Heinrich events, *Paleoceanography*, 20(2), n/a–n/a, doi:10.1029/2004PA001051, 2005.
- 886 Sarnocchia, S., Gasparini, G. P., Astraldi, M., Borghini, M. and Pistek, P.: Dynamics and mixing of the Eastern
887 Mediterranean outflow in the Tyrrhenian basin, *J. Mar. Syst.*, 20(1-4), 301–317, doi:10.1016/S0924-
888 7963(98)00088-8, 1999.
- 889 Spivack, A. J. and Wasserburg, G. J.: Neodymium isotopic composition of the Mediterranean outflow and the
890 eastern North Atlantic, *Geochim. Cosmochim. Acta*, 52(12), 2767–2773, doi:10.1016/0016-7037(88)90144-5,
891 1988.
- 892 Struiver, M., Reimer, P. J. and Reimer, R.: CALIB 7.0, *Radiocarb. Calibration Progr.*, 2005.
- 893 Tachikawa, K., Roy-Barman, M., Michard, A., Thouron, D., Yeghicheyan, D. and Jeandel, C.: Neodymium
894 isotopes in the Mediterranean Sea: comparison between seawater and sediment signals, *Geochim. Cosmochim.
895 Acta*, 68(14), 3095–3106, doi:10.1016/j.gca.2004.01.024, 2004.
- 896 Tachikawa, K., Piotrowski, A. M. and Bayon, G.: Neodymium associated with foraminiferal carbonate as a



- 897 recorder of seawater isotopic signatures, *Quat. Sci. Rev.*, 88, 1–13, doi:10.1016/j.quascirev.2013.12.027, 2014.
- 898 Tanaka, T., Togashi, S., Kamioka, H., Amakawa, H., Kagami, H., Hamamoto, T., Yuhara, M., Orihashi, Y.,
899 Yoneda, S., Shimizu, H., Kunimaru, T., Takahashi, K., Yanagi, T., Nakano, T., Fujimaki, H., Shinjo, R.,
900 Asahara, Y., Tanimizu, M. and Dragusanu, C.: JNdI-1: a neodymium isotopic reference in consistency with
901 LaJolla neodymium, *Chem. Geol.*, 168(3-4), 279–281, doi:10.1016/S0009-2541(00)00198-4, 2000.
- 902 Tachikawa, K., Vidal, L., Cornuault, M., Garcia, M., Pothin, A., Sonzogni, C., Bard, E., Menot, G. and Revel,
903 M.: Eastern Mediterranean Sea circulation inferred from the conditions of S1 sapropel deposition, *Clim. Past*,
904 11(6), 855–867, doi:10.5194/cp-11-855-2015, 2015.
- 905 Taviani, M., Angeletti, L., Canese, S., Cannas, R., Cardone, F., Cau, A., Cau, A. B., Follesa, M. C., Marchese,
906 F., Montagna, P. and Tessarolo, C.: The “Sardinian cold-water coral province” in the context of the
907 Mediterranean coral ecosystems, *Deep Sea Res. Part II Top. Stud. Oceanogr.*, doi:10.1016/j.dsr2.2015.12.008,
908 2015.
- 909 Thunell, R. C. and Williams, D. F.: Glacial–Holocene salinity changes in the Mediterranean Sea: hydrographic
910 and depositional effects, *Nature*, 338(6215), 493–496, doi:10.1038/338493a0, 1989.
- 911 Toucanne, S., Jouet, G., Ducassou, E., Bassetti, M. A., Dennielou, B., Angue Minto'o, C. M., Lahmi, M.,
912 Touyet, N., Charlier, K., Lercolais, G. and Mulder, T.: A 130,000-year record of Levantine Intermediate Water
913 flow variability in the Corsica Trough, western Mediterranean Sea, *Quat. Sci. Rev.*, 33, 55–73,
914 doi:10.1016/j.quascirev.2011.11.020, 2012.
- 915 Vance, D., Scrivner, A. E. and Beney, P.: The use of foraminifera as a record of the past neodymium isotope
916 composition of seawater, *Paleoceanography*, 19(2), PA2009, doi:10.1029/2003PA000957, 2004.
- 917 van de Flierdt, T., Robinson, L. F. and Adkins, J. F.: Deep-sea coral aragonite as a recorder for the neodymium
918 isotopic composition of seawater, *Geochim. Cosmochim. Acta*, 74(21), 6014–6032,
919 doi:10.1016/j.gca.2010.08.001, 2010.
- 920 Voelker, A. H. L., Lebreiro, S. M., Schönfeld, J., Cacho, I., Erlenkeuser, H. and Abrantes, F.: Mediterranean
921 outflow strengthening during northern hemisphere coolings: A salt source for the glacial Atlantic?, *Earth Planet.
922 Sci. Lett.*, 245, 39–55, doi:10.1016/j.epsl.2006.03.014, 2006.
- 923 Weaver, A. J., Saenko, O. a., Clark, P. U. and Mitrovica, J. X.: Meltwater Pulse 1A from Antarctica as a Trigger
924 of the Bolling-Allerod Warm Interval, *Science* (80-.), 299(5613), 1709–1713, doi:10.1126/science.1081002,
925 2003.
- 926 Weldeab, S., Emeis, K.-C., Hemleben, C. and Siebel, W.: Provenance of lithogenic surface sediments and
927 pathways of riverine suspended matter in the Eastern Mediterranean Sea: evidence from $^{143}\text{Nd}/^{144}\text{Nd}$ and
928 $^{87}\text{Sr}/^{86}\text{Sr}$ ratios, *Chem. Geol.*, 186(1-2), 139–149, doi:10.1016/S0009-2541(01)00415-6, 2002.
- 929 Weldeab, S., Menke, V. and Schmiedl, G.: The pace of East African monsoon evolution during the Holocene,
930 *Geophys. Res. Lett.*, 41, 1724–1731, doi:10.1002/2014GL059361. Received, 2014.



- 931 Wienberg, C., Frank, N., Mertens, K. N., Stuut, J.-B. W., Marchant, M., Fietzke, J., Mienis, F. and Hebbeln, D.:
932 Glacial cold-water coral growth in the Gulf of Cádiz: Implications of increased palaeo-productivity, *Earth*
933 *Planet. Sci. Lett.*, 298(3-4), 405–416, doi:10.1016/j.epsl.2010.08.017, 2010.

934 Wu, Q., Colin, C., Liu, Z., Thil, F., Dubois-Dauphin, Q., Frank, N., Tachikawa, K., Bordier, L. and Douville, E.:
935 Neodymium isotopic composition in foraminifera and authigenic phases of the South China Sea sediments:
936 Implications for the hydrology of the North Pacific Ocean over the past 25 kyr, *Geochemistry, Geophys.*
937 *Geosystems*, 16(11), 3883–3904, doi:10.1002/2015GC005871, 2015.

938 **Table captions**

939

940 **Table 1.** U-series ages and ε_{Nd} values obtained for cold-water coral samples collected from sediment core RECORD 23
941 (Sardinia Channel).

942

943 **Table 2.** ε_{Nd} values obtained for cold-water corals from the southern Alboran Sea. The AMS ^{14}C ages published by Fink et
944 al. (2013) are also reported as Median probability age (ka BP).

945

946 **Table 3.** AMS ^{14}C ages of samples of the planktonic foraminifer *G. bulloides* from ‘off-mound’ sediment core SU92-33. The
947 AMS ^{14}C ages were corrected for ^{13}C and a mean reservoir age of 400 yrs, and were converted into calendar years using the
948 INTCAL13 calibration data set (Reimer et al., 2013) and the CALIB 7.0 program (Struiver et al., 2005).

949

950 **Table 4.** Multiproxy data obtained for the upper 2.1 m of sediment core SU92-33 (Balearic Sea). Stable oxygen and carbon
951 isotopes were measured on benthic (*C. pachyderma*) and planktonic (*G. bulloides*) foraminifera; ε_{Nd} values were obtained on
952 mixed planktonic foraminifera samples. The age results from a combination of 7 AMS- ^{14}C age measurements for the upper
953 1.2 m of the core and by a linear interpolation between these ages as well as the $\delta^{18}\text{O}$ variations of the planktonic
954 foraminifera *G. bulloides*.

955

956 **Figure captions**

957

958 **Figure 1.** Map of the western Mediterranean Sea showing the locations of samples investigated in this study. Yellow dot
959 indicates the sampling location of the sediment core from the Balearic Sea (SU92-33); yellow stars indicate the locations of
960 the CWC-bearing cores from the Sardinia Channel (RECORD 23) and the southern Alboran Sea (for further details on the
961 CWC from the Alboran Sea refer also to Fink et al., 2013). The cores discussed in this paper (Gulf of Cádiz: IODP site
962 U1387, Balearic Sea: MD09-2343, northern Tyrrhenian Sea: MD01-2472, Adriatic Sea: MD90-917) are indicated by black
963 dots, and seawater stations are marked by open squares. Arrows represent the main oceanographic currents. The black line
964 shows the general trajectory of the Modified Atlantic Water (MAW) flowing at the surface from the Atlantic Ocean toward
965 the western and eastern Mediterranean. The orange line represents the Levantine Intermediate Water (LIW) originating from
966 the eastern basin. The black dashed line shows the trajectory of the Western Mediterranean Deep Water (WMDW) flowing
967 from the Gulf of Lions toward the Strait of Gibraltar.

968

969 **Figure 2.** (a) Sea Surface Temperature (SST) records of cores SU92-33 (red line) and MD90-917 (green line), (b) $\delta^{18}\text{O}$
970 record obtained on planktonic foraminifer *G. bulloides* for core SU92-33, (c) $\delta^{18}\text{O}$ record obtained on benthic foraminifer *C.*
971 *pachyderma* for core SU92-33, (d) $\delta^{13}\text{C}$ record obtained on benthic foraminifer *C. pachyderma* for core SU92-33. LGM: Last



972 Glacial Maximum; HS1: Heinrich Stadial 1; B-A: Bølling-Allerød; YD: Younger Dryas. Black triangles indicate AMS ^{14}C
973 age control points.

974

975 **Figure 3.** (a) Sea Surface Temperature (SST) record of core SU92-33 (red line), (b) εNd records obtained on mixed
976 planktonic foraminifers from core SU92-33 (open circles) and from cold-water coral fragments collected in the Alboran Sea
977 (red squares), (c) εNd values of cold-water corals from core RECORD 23 (Sardinia Channel).

978

979 **Figure 4.** (a) $\delta^{13}\text{C}$ records obtained on benthic foraminifer *C. pachyderma* for cores SU92-33 (red line) and MD99-2343
980 (blue line; Sierro et al., 2005). (b) εNd records obtained on mixed planktonic foraminifers from core SU92-33 (open circles)
981 and from cold-water coral fragments collected in the Alboran Sea (red squares). Modern εNd values for LIW (orange dashed
982 line) and WMDW (blue dashed line) are also reported for comparison. (c) εNd values obtained for planktonic foraminifera
983 with Fe-Mn coatings at sites 300G ($36^{\circ}21.532'$ N, $1^{\circ}47.507'$ W; 1860 m; open dots) and 304G ($36^{\circ}19.873'$ N, $1^{\circ}31.631'$ W;
984 2382 m; black dots) in Alboran Sea (Jimenez-Espejo et al., 2015). (d) UP10 fraction ($>10 \mu\text{m}$) from core MD99-2343
985 (Frigola et al., 2008). (e) Sortable silt mean grain-size of core MD01-2472 (Toucanne et al., 2012). (f) Ln Zr/Al ratio at IODP
986 site U1387 ($36^{\circ}48.3'$ N $7^{\circ}43.1'$ W; 559 m) (Bahr et al., 2015).

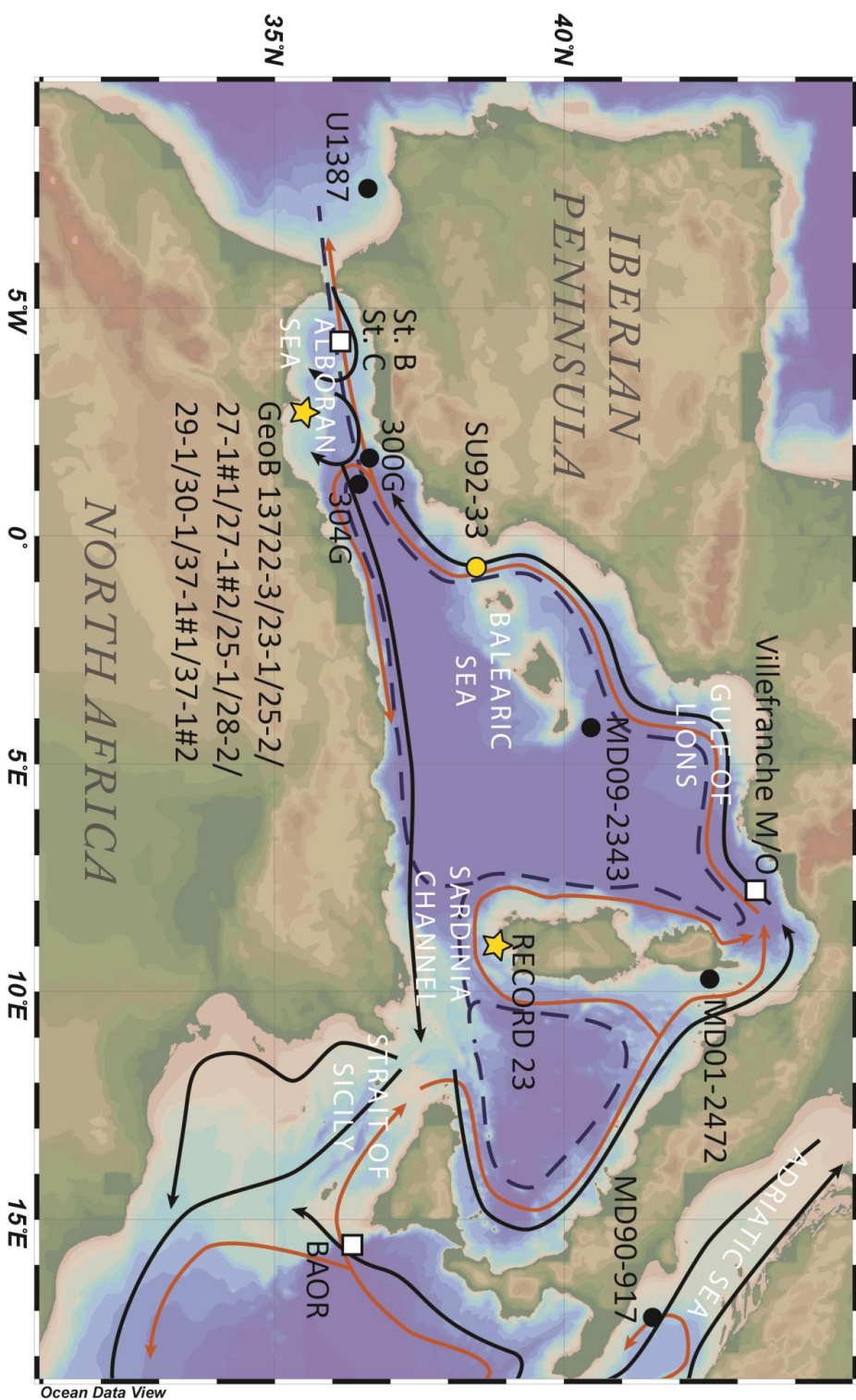
987

988 **Figure 5.** (a) $\delta^{18}\text{O}$ record obtained on planktonic foraminifer *G. bulloides* for core SU92-33, (b) $\delta^{13}\text{C}$ records obtained on
989 benthic foraminifer *C. pachyderma* for core SU92-33, (c) εNd values of cold-water corals from core RECORD 23 (Sardinia
990 Channel), (d) εNd values records obtained on mixed planktonic foraminifera from core SU92-33 (open circles) and from
991 cold-water coral fragments collected in the Alboran Sea (red squares), (e) εNd values obtained on terrigenous fraction of
992 MS27PT located close the Nile River mouth in the eastern Mediterranean basin (Revel et al., 2015).

993



Figure 1



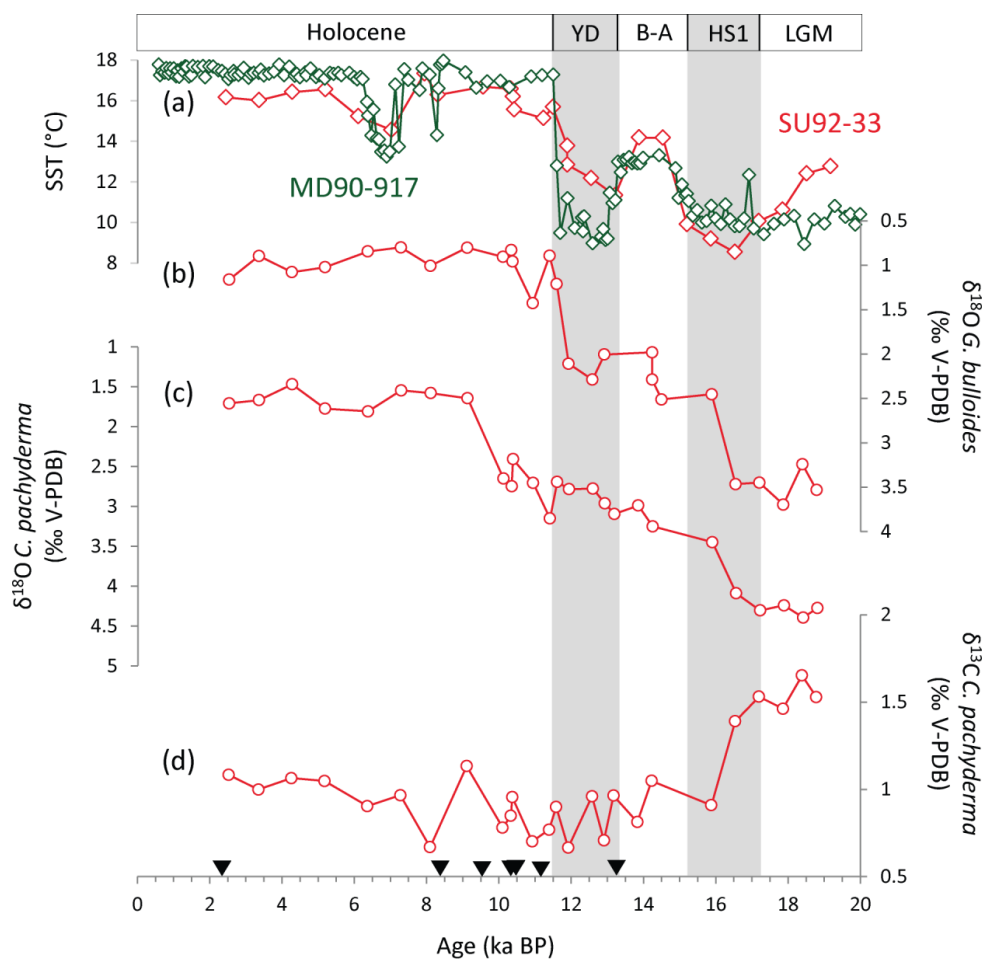


Figure 2

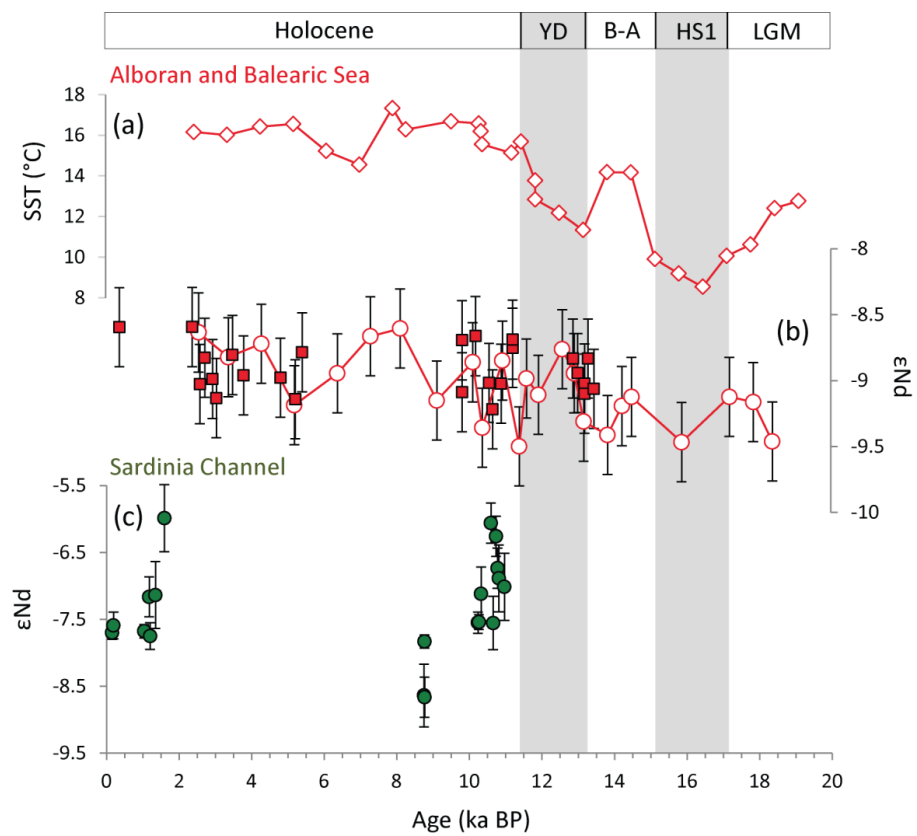


Figure 3

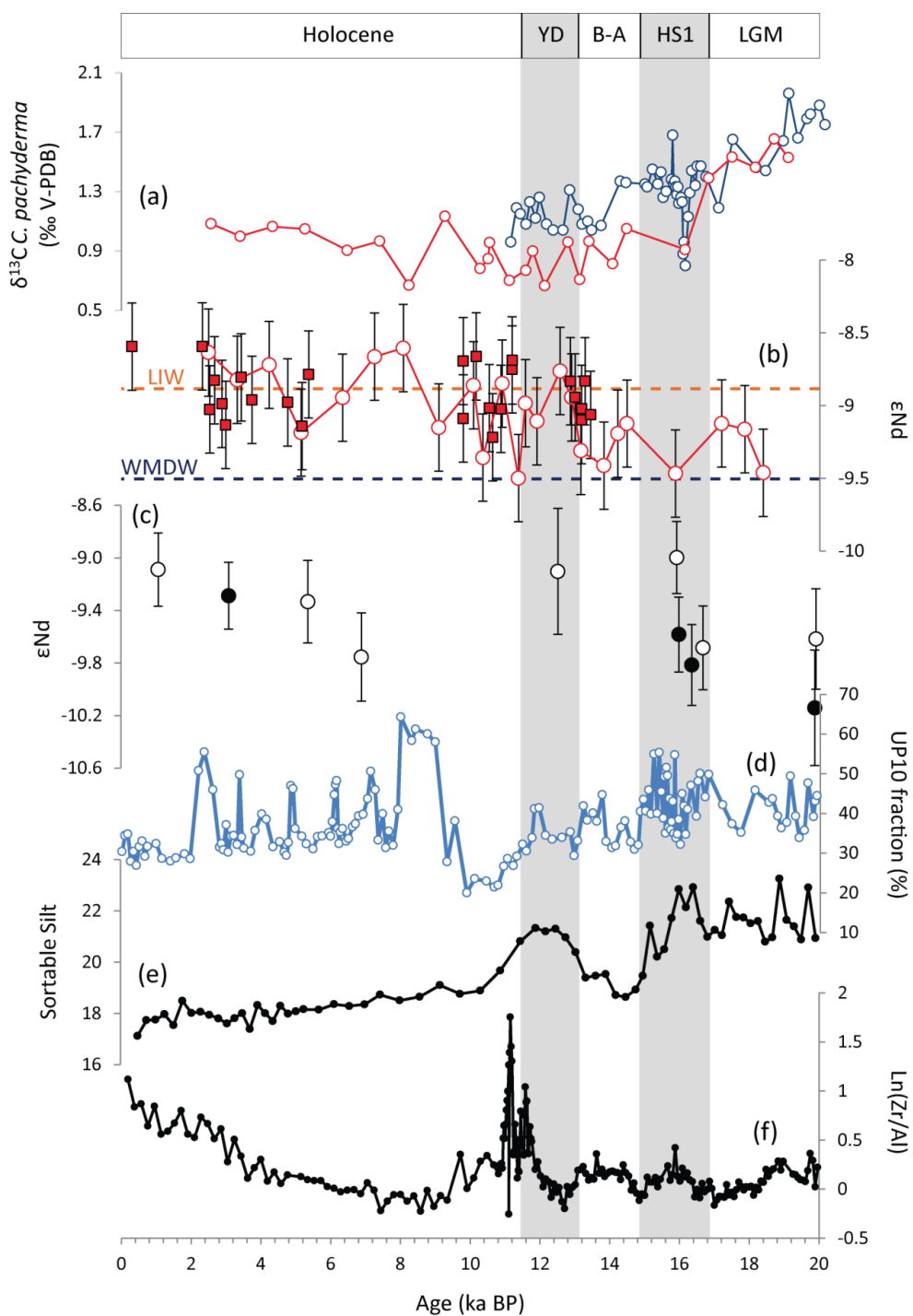


Figure 4

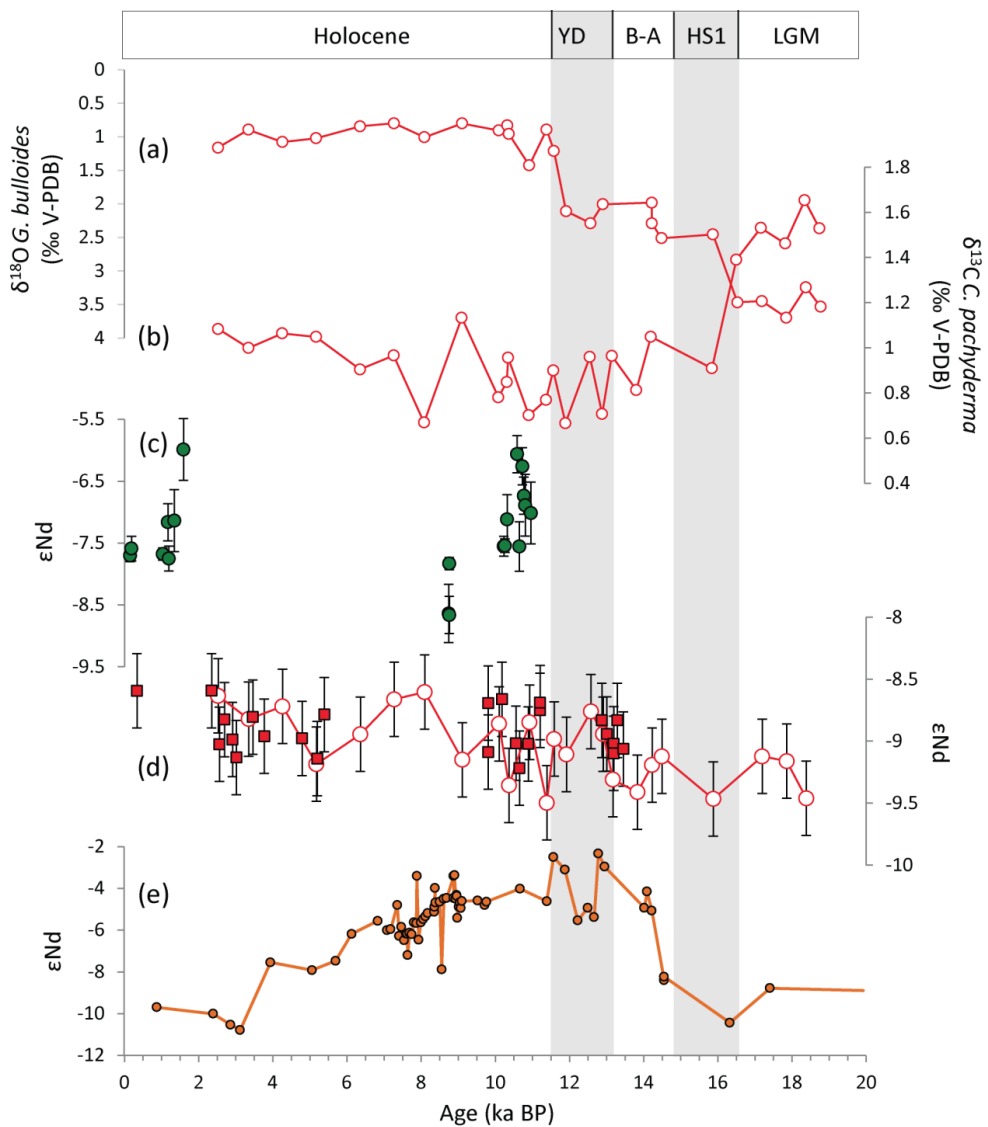


Figure 5



Sample ID	Depth in core (cm)	Corals species	^{238}U ($\mu\text{g/g}$)	^{232}Th (ng/g)	$\delta^{234}\text{U}_{\text{in}}$ (‰)	$^{230}\text{Th}/^{238}\text{U}$	$^{230}\text{Th}/^{232}\text{Th}$	Age (ka BP)	$\delta^{231}\text{U}_{\text{D}}$ (‰)	$^{143}\text{Nd}/^{144}\text{Nd}$	ϵNd
RECORD_23_V	0-3.5	<i>Madrepora oculata</i>	3.31 ±0.005	0.68 ±0.014	151.85 ±1.7	0.00163 ±0.00011	25 ±1.7	0.091 ±0.011	151.92 ±1.7	0.512243 ±0.000005	-7.70 ±0.10
RECORD_23_V	3-7	<i>Madrepora oculata</i>	3.23 ±0.002	0.52 ±0.001	147.11 ±0.6	0.00159 ±0.00006	38 ±1.1	0.127 ±0.006	147.19 ±0.6	0.512249 ±0.000010	-7.59 ±0.20
RECORD_23_V	7-10	<i>Madrepora oculata</i>	3.99 ±0.007	0.25 ±0.002	147.52 ±1.7	0.00127 ±0.00022	640 ±11.6	1.110 ±0.023	148.01 ±1.7	0.512244 ±0.000015	-7.58 ±0.30
RECORD_23_V	8-10	<i>Madrepora oculata</i>	3.79 ±0.005	0.41 ±0.001	147.77 ±0.7	0.001253 ±0.00007	350 ±2.0	1.135 ±0.008	148.27 ±0.7	0.512271 ±0.000010	-7.16 ±0.20
RECORD_23_IV	6-9	<i>Madrepora oculata</i>	4.06 ±0.006	0.35 ±0.001	148.47 ±1.2	0.001366 ±0.00011	480 ±3.8	1.243 ±0.012	149.02 ±1.2	0.512241 ±0.000010	-7.75 ±0.20
RECORD_23_IV	27-30	<i>Madrepora oculata</i>	4.06 ±0.003	1.09 ±0.001	146.91 ±1.3	0.001405 ±0.00013	159 ±1.4	1.283 ±0.014	147.47 ±1.3	0.512272 ±0.000026	-7.14 ±0.50
RECORD_23_IV	37-40	<i>Madrepora oculata</i>	3.52 ±0.005	0.08 ±0.000	142.25 ±1.1	0.001663 ±0.00012	2308 ±16.4	1.529 ±0.013	148.92 ±1.1	0.512331 ±0.000026	-5.99 ±0.50
RECORD_23_III	55-57	<i>Madrepora oculata</i>	3.63 ±0.002	0.27 ±0.000	145.30 ±0.7	0.008332 ±0.000020	3530 ±8.1	8.685 ±0.027	148.93 ±0.8	0.512195 ±0.000026	-8.64 ±0.50
RECORD_23_III	58-61	<i>Madrepora oculata</i>	4.24 ±0.004	0.36 ±0.001	145.71 ±1.2	0.008359 ±0.000037	3336 ±14.0	8.702 ±0.048	150.39 ±1.2	0.512237 ±0.000010	-7.83 ±0.20
RECORD_23_III	63-66	<i>Lophelia pertusa</i>	4.15 ±0.005	0.42 ±0.002	147.19 ±0.8	0.008363 ±0.000054	2783 ±17.1	8.703 ±0.063	150.89 ±0.9	0.512194 ±0.000015	-8.66 ±0.30
RECORD_23_I	0-2	<i>Lophelia pertusa</i>	3.35 ±0.002	0.37 ±0.000	147.02 ±0.7	0.00283 ±0.00018	2788 ±4.8	10.173 ±0.025	151.34 ±0.7	0.512251 ±0.000010	-7.55 ±0.20
RECORD_23_I	62-65	<i>Lophelia pertusa</i>	3.27 ±0.003	0.39 ±0.002	144.75 ±1.2	0.00289 ±0.00061	2721 ±16.1	10.201 ±0.075	149.01 ±1.2	0.512251 ±0.000010	-7.54 ±0.20
RECORD_23_II	50-52	<i>Lophelia pertusa</i>	2.92 ±0.003	0.92 ±0.003	145.39 ±1.6	0.010351 ±0.00061	1046 ±6.2	10.260 ±0.079	149.69 ±1.6	0.512273 ±0.000021	-7.12 ±0.40
RECORD_23_II	12-14	<i>Lophelia pertusa</i>	3.07 ±0.002	0.49 ±0.000	145.22 ±0.7	0.010609 ±0.00023	1971 ±4.3	10.531 ±0.031	149.64 ±0.7	0.512327 ±0.000015	-6.06 ±0.30
RECORD_23_II	5-7	<i>Lophelia pertusa</i>	3.50 ±0.002	0.42 ±0.000	146.35 ±0.9	0.010677 ±0.00016	2654 ±4.0	10.591 ±0.025	150.82 ±0.9	0.512251 ±0.000021	-7.55 ±0.40
RECORD_23_II	94-98	<i>Lophelia pertusa</i>	3.14 ±0.003	0.62 ±0.002	146.42 ±1.0	0.010755 ±0.00047	1737 ±7.6	10.672 ±0.059	150.94 ±1.0	0.512317 ±0.000015	-6.26 ±0.30
RECORD_23_I	15-17	<i>Lophelia pertusa</i>	3.40 ±0.003	0.46 ±0.000	145.01 ±0.9	0.010790 ±0.00021	2409 ±4.6	10.713 ±0.031	150.53 ±0.9	0.512293 ±0.000015	-6.73 ±0.30
RECORD_23_II	96-100	<i>Lophelia pertusa</i>	3.61 ±0.004	0.35 ±0.001	145.50 ±0.8	0.010821 ±0.00044	3579 ±14.7	10.750 ±0.055	150.02 ±0.8	0.512285 ±0.000026	-6.89 ±0.50
RECORD_23_II	93-95	<i>Lophelia pertusa</i>	3.19 ±0.003	0.24 ±0.000	143.33 ±0.8	0.010947 ±0.00032	4381 ±12.7	10.904 ±0.042	147.85 ±0.9	0.512279 ±0.000026	-7.01 ±0.50

Table 1



Sample ID	Core depth (cm)	Species	Water Depth (m)	Median probability age (ka BP)	$^{143}\text{Nd}/^{144}\text{Nd}$	ϵNd
GeoB 13727-1#1	Surface	<i>Lophelia pertusa</i>	363	0.339	0.512198 ±0.000015	-8.59 ±0.30
GeoB 13727-1#2	Surface	<i>Madrepora oculata</i>	353	2.351	0.512198 ±0.000015	-8.59 ±0.30
GeoB 13730-1	6	<i>Lophelia pertusa</i>	338	2.563	0.512175 ±0.000015	-9.03 ±0.30
GeoB 13728-1	Bulk (0-15)	<i>Lophelia pertusa</i>	343	2.698	0.512185 ±0.000015	-8.83 ±0.30
GeoB 13728-2	2	<i>Lophelia pertusa</i>	343	2.913	0.512177 ±0.000015	-8.99 ±0.30
GeoB 13722-3	Bulk (0-15)	<i>Madrepora oculata</i>	280	3.018	0.512170 ±0.000015	-9.13 ±0.30
GeoB 13722-3	Bulk (15-30)	<i>Madrepora oculata</i>	280	3.463	0.512186 ±0.000015	-8.81 ±0.30
GeoB 13735-1	Bulk (0-15)	<i>Madrepora oculata</i>	280	3.770	0.512179 ±0.000015	-8.96 ±0.30
GeoB 13723-1	Bulk (0-8)	<i>Madrepora oculata</i>	291	4.790	0.512178 ±0.000015	-8.98 ±0.30
GeoB 13725-2	Surface	<i>Madrepora oculata</i>	355	5.201	0.512169 ±0.000015	-9.14 ±0.30
GeoB 13723-1	Bulk (8-20)	<i>Madrepora oculata</i>	291	5.390	0.512187 ±0.000015	-8.79 ±0.30
GeoB 13729-1	2.5	<i>Lophelia pertusa</i>	442	9.810	0.512172 ±0.000015	-9.09 ±0.30
GeoB 13729-1	2.5	<i>Lophelia pertusa</i>	442	9.810	0.512193 ±0.000015	-8.69 ±0.30
GeoB 13729-1	49	<i>Lophelia pertusa</i>	442	10.181	0.512194 ±0.000015	-8.66 ±0.30
GeoB 13730-1	102	<i>Lophelia pertusa</i>	338	10.556	0.512176 ±0.000015	-9.02 ±0.30
GeoB 13730-1	194	<i>Lophelia pertusa</i>	338	10.652	0.512165 ±0.000015	-9.22 ±0.30
GeoB 13729-1	315	<i>Lophelia pertusa</i>	442	10.889	0.512176 ±0.000015	-9.02 ±0.30
GeoB 13729-1	375	<i>Lophelia pertusa</i>	442	11.206	0.512189 ±0.000015	-8.75 ±0.30
GeoB 13730-1	298	<i>Lophelia pertusa</i>	338	11.208	0.512193 ±0.000015	-8.69 ±0.30
GeoB 13728-2	191	<i>Lophelia pertusa</i>	343	12.874	0.512185 ±0.000015	-8.83 ±0.30
GeoB 13737-1#2	Surface	<i>Lophelia pertusa</i>	297	13.005	0.512180 ±0.000015	-8.94 ±0.30
GeoB 13728-2	295	<i>Lophelia pertusa</i>	364	13.194	0.512176 ±0.000015	-9.02 ±0.30
GeoB 13728-2	295	<i>Lophelia pertusa</i>	364	13.194	0.512171 ±0.000015	-9.10 ±0.30
GeoB 13730-1	427	<i>Lophelia pertusa</i>	338	13.291	0.512185 ±0.000015	-8.83 ±0.30
GeoB 13737-1#1	Surface	<i>Lophelia pertusa</i>	299	13.452	0.512174 ±0.000015	-9.06 ±0.30

Table 2



Core	Depth in core (cm)	^{14}C -age (years)	$\pm 1\sigma$ (years)	Median probability age (ka BP)
SU92-33	0	2770	70	2437
SU92-33	64	7870	90	8280
SU92-33	70	8670	80	9528
SU92-33	74	9510	100	10295
SU92-33	84	9610	90	10389
SU92-33	90	10180	100	11192
SU92-33	120	11710	110	13172

Table 3



Depth in core (cm)	Age (ka BP)	$\delta^{13}\text{C}$ <i>C. pachyderma</i> (‰ VPDB)	$\delta^{18}\text{O}$ <i>C. pachyderma</i> (‰ VPDB)	$\delta^{13}\text{C}$ <i>G. bulloides</i> (‰ VPDB)	$\delta^{18}\text{O}$ <i>G. bulloides</i> (‰ VPDB)	$^{143}\text{Nd}/^{144}\text{Nd}$	ϵNd
1	2.53	1.08	1.71	-0.6	1.16	0.512195 ± 0.000015	-8.64 ± 0.30
10	3.35	1.00	1.67	-0.82	0.90	0.512186 ± 0.000015	-8.82 ± 0.30
19.5	4.26	1.06	1.47	-0.55	1.08	0.512191 ± 0.000015	-8.72 ± 0.30
29.5	5.18	1.05	1.78	-0.55	1.02	0.512167 ± 0.000015	-9.19 ± 0.30
42.5	6.36	0.90	1.81	-0.91	0.84	0.512179 ± 0.000015	-8.95 ± 0.30
52.5	7.28	0.97	1.55	-0.80	0.80	0.512194 ± 0.000015	-8.66 ± 0.30
61.5	8.10	0.67	1.58	-0.95	1.01	0.512197 ± 0.000015	-8.61 ± 0.30
67.5	9.11	1.13	1.65	-1.07	0.80	0.512169 ± 0.000015	-9.15 ± 0.30
72.5	10.10	0.78	2.65	-1.27	0.91	0.512184 ± 0.000015	-8.86 ± 0.30
77.5	10.33	0.85	2.75	-1.10	0.83	-	-
81.5	10.37	0.96	2.41	-1.21	0.96	0.512158 ± 0.000015	-9.36 ± 0.30
87.5	10.92	0.70	2.71	-0.11	1.43	0.512184 ± 0.000015	-8.85 ± 0.30
92.5	11.39	0.77	3.15	-1.00	0.89	0.512151 ± 0.000015	-9.50 ± 0.30
95.5	11.59	0.90	2.69	-1.14	1.21	0.512178 ± 0.000015	-8.98 ± 0.30
100.5	11.92	0.67	2.78	-0.44	2.11	0.512171 ± 0.000015	-9.11 ± 0.30
110.5	12.58	0.96	2.78	-0.86	2.29	0.512189 ± 0.000015	-8.76 ± 0.30
115.5	12.91	0.71	2.96	-0.54	2.01	0.512180 ± 0.000015	-8.94 ± 0.30
119.5	13.17	0.96	3.09	-	-	0.512161 ± 0.000015	-9.31 ± 0.30
129.5	13.83	0.81	2.99	-	-	0.512156 ± 0.000015	-9.41 ± 0.30
135.5	14.23	1.05	3.25	-1.16	1.98	0.512167 ± 0.000015	-9.19 ± 0.30
135.5	14.23	-	-	-0.94	2.29	-	-
139.5	14.49	-	-	-0.96	2.51	0.512170 ± 0.000015	-9.12 ± 0.30
159.5	15.88	0.91	3.45	-0.81	2.45	0.512153 ± 0.000015	-9.47 ± 0.30
169.5	16.54	1.39	4.09	-0.76	3.47	-	-
179.5	17.20	1.53	4.30	-0.98	3.45	0.512170 ± 0.000015	-9.12 ± 0.30
190	17.86	1.46	4.24	-1.10	3.70	0.512168 ± 0.000015	-9.16 ± 0.30
198	18.39	1.65	4.39	-1.24	3.24	0.512153 ± 0.000015	-9.46 ± 0.30
206	18.78	1.53	4.28	-0.90	3.53	-	-

Table 4